Quaternary Science Reviews 34 (2012) 127–145

Contents lists available at SciVerse ScienceDirect

Quaternary Science Reviews

journal homepage: www.elsevier.com/locate/quascirev

# Evolution of an overdeepened trough in the northern Alpine Foreland at Niederweningen, Switzerland

Andreas Dehnert [a,*], Sally E. Lowick [b], Frank Preusser [b,1], Flavio S. Anselmetti [c], Ruth Drescher-Schneider [d], Hans Rudolf Graf [e], Friedrich Heller [f], Heinrich Horstmeyer [g], Hans Axel Kemna [a,2], Norbert R. Nowaczyk [h], Andreas Züger [i], Heinz Furrer [a]

[a] Palaeontological Institute and Museum, University of Zurich, Karl-Schmid-Strasse 4, 8006 Zurich, Switzerland
[b] Institute of Geological Sciences, University of Bern, Baltzerstrasse 1+3, 3012 Bern, Switzerland
[c] Eawag, Swiss Federal Institute of Aquatic Science and Technology, Überlandstrasse 133, P.O. Box 611, 8600 Dübendorf, Switzerland
[d] Institute of Plant Sciences, Karl-Franzens University of Graz, Holteigasse 6, 8010 Graz, Austria
[e] Matousek, Baumann & Niggli AG, Mäderstrasse 8, 5401 Baden, Switzerland
[f] Institute of Geophysics, ETH Zurich, Sonneggstr. 5, 8092 Zurich, Switzerland
[g] AUGEOS GmbH, Meisenweg 1, 8038 Zurich, Switzerland
[h] Helmholz Centre Potsdam, GFZ German Research Centre for Geosciences, Telegrafenberg C 321, 14473 Potsdam, Germany
[i] Oeschger Centre for Climate Change Research, University of Bern, Zähringerstrasse 25, 3012 Bern, Switzerland

ARTICLE INFO

*Article history:*
Received 12 September 2011
Received in revised form
14 December 2011
Accepted 16 December 2011
Available online 21 January 2012

*Keywords:*
Glacial overdeepening
MIS 6
Sediment core
Pollen analysis
Luminescence dating

ABSTRACT

Quaternary deposits in the overdeepened Wehntal, Switzerland, were investigated using both seismic profiling and the analysis of 93.6 m long drill core using sedimentology, geochemistry, palynology, magnetic properties, and luminescence dating. The sediments reveal evidence for two glacial advances that reached the area during Marine Isotope Stage (MIS) 6. The first advance (~185 ka) may have carved out the basin or at least removed the entire previous Quaternary sediment filling. This first advance likely reached far beyond the limit of the maximum of the Last Glaciation. The second advance (~140 ka) was of smaller extent, possibly of cold-based nature, and likely reached only slightly beyond the limits of the Last Glaciation.



## 1. Introduction

Repeated glaciations during the Quaternary have had a large impact on the morphology of the Alpine foreland. Geophysical surveys and deep drillings have revealed the existence of deep erosional structures filled mainly by glacial sediments (Dürst Stucki et al., 2010; Jordan, 2010; Preusser et al., 2010). These features, found below many perialpine valleys and below almost every major lake basin, are commonly referred to as overdeepened valleys and basins. The buried troughs are interpreted as having been formed by subglacial processes, i.e. by a combination of abrasion and glacial meltwater erosion (cf. Dürst Stucki et al., 2010; Preusser et al., 2010). The mechanisms and timing of glacial erosion in the northern Alpine foreland were discussed in the 1970s (e.g. Schlüchter, 1979), but received little further attention until recently, when they became relevant to the long-term safety evaluation regarding the planning of a deep geological nuclear-waste repository site in Switzerland. The timing of glacial overdeepening is of major importance in this context, but has been poorly constrained so far.

The oldest dated sedimentary filling of a trough in the northern Swiss Alpine foreland is located well within the limits of the Last Glaciation (Würmian) referred to as the Birrfeld Glaciation in northern Switzerland (Graf, 2009). The basal part of this sequence at Thalgut (Schlüchter, 1989a,b, Fig. 1A) comprises lacustrine sediments bearing an interglacial pollen assemblage with a dominance of *Fagus* (up to 58%) and up to 7% of *Pterocarya* pollen (Welten, 1988), considered to represent the Holsteinian interglacial (cf. de Beaulieu et al., 2001). The age of the Holsteinian is, however,

* Corresponding author. Present address: Swiss Federal Nuclear Safety Inspectorate ENSI, Industriestrasse 19, 5200 Brugg, Switzerland. Tel.: +41 56 460 8640.
*E-mail address:* andreas.dehnert@ensi.ch (A. Dehnert).
[1] Present address: Department of Physical Geography and Quaternary Geology, Stockholm University, 10691 Stockholm, Sweden.
[2] Present address: Ucon Geoconsulting, Breite Strasse 67, 47798 Krefeld, Germany.

0277-3791/$ – see front matter © 2012 Elsevier Ltd. All rights reserved.
doi:10.1016/j.quascirev.2011.12.015

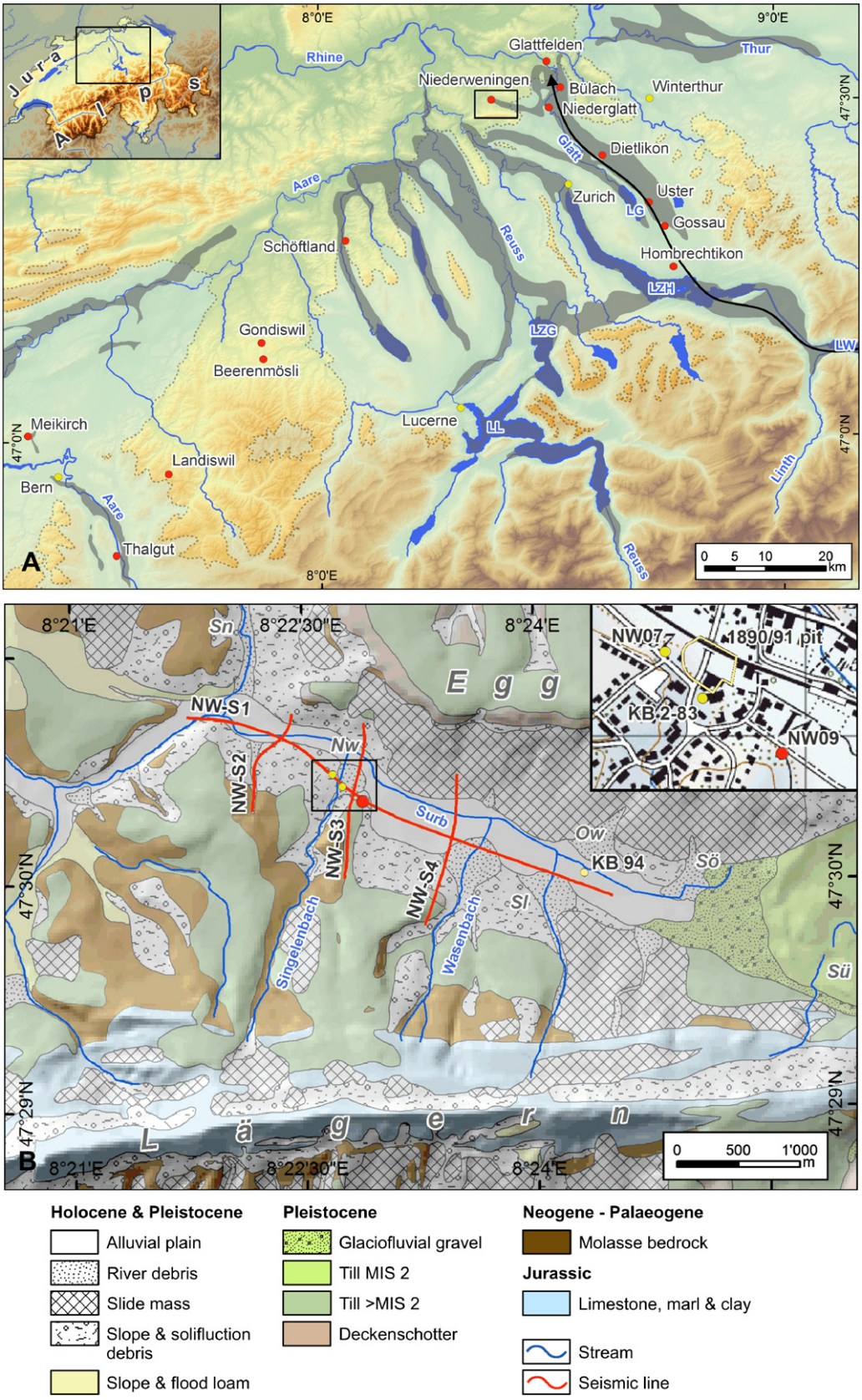


**Fig. 1.** A) Overview of the Swiss Alpine Foreland with the drill site Niederweningen and other localities mentioned in the text (red dots). Alpine glacier extent during the Last Glacial Maximum (dotted line, adopted from Bini et al. (2009)), main Walensee Glacier flow path (back arrow), and approximate locations of overdeepened troughs (grey areas, after Jordan (2010), Jordan et al. (2008), Pugin (1988), and Wildi (1984)) are further indicated. Abbreviations of lakes: LL Lake Lucerne, LZG Lake Zug, LZH Lake Zurich, LG Greifensee, LW Lake Walen (Walensee). Coordinates are given in WGS84. Inset in top left corner shows location of Fig. 1A within Switzerland. (B) Geological map of the Wehntal area with coring location of NW09 (red dot) and KB 94 (Graf and Müller, 1999). Inset in top right corner is a zoom to the village of Niederweningen showing locations of older important study sites such as the mammoth pit of 1890/91 (Lang, 1892) and the coring locations of KB 2–83 (Welten, 1988) and NW07 (Anselmetti et al., 2010). Coordinates are in WGS84. Abbreviations of villages mentioned in the text: Sn Schneisingen, Nw Niederweningen, Sl Schleinikon, Ow Oberweningen, Sö Schöfflisdorf, Sü Sünikon.

controversial, with de Beaulieu et al. (2001) correlating it with Marine Isotope Stage (MIS; all given age ranges according to Bassinot et al. (1994)) 11 (427–364 ka), while Geyh and Müller (2005) correlate it with MIS 9 (334–301 ka) following U/Th dates on peat in its type region in northern Germany. As a consequence, the glaciation that formed the Thalgut trough is assigned to either MIS 12 (474–427 ka) or MIS 10 (364–334 ka), providing a minimum age for the overdeepening process. The Meikirch drill site, also situated within the limits of the Last Glaciation, provides a 112 m-long sequence of lacustrine sediments overlain by glacial deposits (Welten, 1982, 1988). Luminescence dating and a re-interpretation of the pollen record by Preusser et al. (2005) indicate that the lake deposits formed during MIS 7 (242–186 ka), implying a minimum MIS 8 age (301–242 ka) for the erosion of the glacial trough.

The Richterswil trough (Rhine-Linth Glacier) between Lake Zurich and Lake Zug shows a maximum depth of ~365 m and is filled by sediments attributed to at least four major glaciations (Blüm and Wyssling, 2007; Wyssling, 2002). It bears two intercalated lake-sediment units, the upper of which is correlated with the Eemian (MIS 5e) by its pollen content. Two almost parallel overdeepened troughs are located in the upper Glatt Valley, north-east of Lake Zurich (Fig. 1A). The Greifensee and the Uster trough are overdeepened, by the Walensee branch of the Rhine-Linth Glacier (in the following referred to as Walensee Glacier) by at least 50 and 130 m, respectively. Molasse bedrock of the deeper Uster trough is overlain by thick glacial and lacustrine deposits, which are tentatively correlated to the Rissian Glaciation (MIS 6, 186–127 ka, also referred to as the Beringen Glaciation (Graf, 2009)) and the Eemian Interglacial (Wyssling and Wyssling, 1978). Further downstream of the River Glatt, the Uster trough merges into the middle Glatt Valley trough, consisting of two parallel sub-basins cut into molasse bedrock. A drillhole into the northern sub-basin near Dietlikon revealed overdeepening of at least 150 m. Similar to the Uster trough, Haldimann (1978) reports basal till deposits overlain by thick laminated lake sediments of this site and also correlates them to the Rissian glaciation and its following interglacial based on stratigraphic correlation. Freimoser and Locher (1980) report 195 m overdeepening of the lower Glatt Valley trough, which displays molasse bedrock topped by basal till and thick lake-sediment sequences. As this basin reaches beyond the ice extent of the Last Glaciation, Freimoser and Locher (1980) argue that the most likely candidate for the overdeepening must be the older Rissian Glaciation.

With regard to the potential age of most of the overdeepened structures mentioned above, it is important to note that controversy surrounds the question of glaciation of the Swiss lowlands during MIS 6. The Rissian Glaciation is usually correlated with the MIS 6 (e.g. van Husen, 2004) and represents an extensive glaciation, substantially beyond the limits of the Last Glaciation. Based on palynological and geological evidence, it, however, has been suggested that MIS 6 glaciers did not reach beyond the border of the Swiss Alps (Schlüchter, 1988b, 2004) and this view has been adopted by many Quaternary stratigraphers in Switzerland, despite considerable contradictory evidence from many other regions. More recently, luminescence dating of proglacial sediments from Landiswil (Dehnert et al., 2010) and cosmogenic nuclide dating of erratic boulders from the Jura Mountains (Graf et al., 2007) imply that glaciers did reach far beyond the limits of the Last Glaciation during MIS 6.

Here, we present the results of a drill core from the overdeepened Wehntal trough at Niederweningen (Fig. 1), where sediments have been studied in detail since the discovery of an important Quaternary vertebrate site in the late 19th century (Lang, 1892). A 30 m deep drill core close to this palaeontological site was previously investigated by Anselmetti et al. (2010). Bedrock however, was not reached by this drilling, and the present study, is based on a core that did reach bedrock. The sedimentological and geochemical composition of the core presented here, and pollen analysis, palaeomagnetic studies, and luminescence dating provide age estimates for the sedimentary filling. These comprehensive analyses provide new insights into the timing and formation history of overdeepened glacial troughs and present new data with regard to the debate concerning the extent of glaciers in the northern Swiss Alpine foreland during MIS 6.

## 2. Regional setting

Wehntal is a ~5 km-long valley (Fig. 1) drained by a small stream named Surb. The east–west alignment follows the orientation of the Lägern anticline structure composed of Jurassic carbonates (mainly shallow-water limestones) that borders the valley to the south. The northern slope of Wehntal, named Egg, is made up of molasse bedrock covered by Early Pleistocene Deckenschotter deposits (Bitterli-Dreher et al., 2007; Graf, 1993). The western end of Wehntal appears gorge-like with molasse hills cut by the Surb. The eastern entrance of the valley is characterised by a terminal moraine ridge formed by a lateral lobe of the Walensee Glacier during the maximum extent of the Last Glaciation (Keller and Krayss, 2005a,b). Periglacial conditions during MIS 2 caused sliding, solifluction, and cryoturbation in many parts of the valley (Fig. 1B), but commonly occurring deeply weathered till patches, that cover large areas of Wehntal and Egg, are mostly likely older than the Last Glaciation. The recent flat valley floor is an alluvial plain formed by the debris of second-order streams, mostly draining the north-facing slope of Lägern. The widening of the valley to its present day size, and its overdeepening into molasse bedrock is suggested to have been forced by Middle Pleistocene glaciers, although the exact time of formation is not known (Bitterli-Dreher et al., 2007).

All discoveries of Pleistocene mammals are related to a shallow buried peat horizon, the so-called 'mammoth peat' (cf. Furrer et al., 2007). Radiocarbon and luminescence dating of this peat and associated sediments indicate an age of ~45 ka (Hajdas et al., 2007, 2009; Preusser and Degering, 2007). Welten (1988), Schlüchter (1988a, 1994), and more recently Anselmetti et al. (2010) demonstrate the presence of a second, deeper buried peat layer. According to pollen stratigraphy of core KB 2–83 (Fig. 1B), Welten (1988) proposed a correlation of the lower peat with the last interglacial (Eemian), which has been confirmed by core NW07 (Anselmetti et al. (2010). Deeper in the core, Welten (1988) identified a further interglacial that he correlated with the Holsteinian, although this correlation now appears inappropriate as neither a dominance of *Fagus* nor a clear presence of *Pterocarya* was been identified in the pollen assemblages. Nevertheless, the absence of glacial sediments between the Eemian and the older interglacial has been used as one argument for the absence of an extensive glaciation during MIS 6 (Schlüchter, 1988b). Anselmetti et al. (2010, Fig. 1B), have shown that the "Eemian peat" unconformably tops a carbonate-rich lacustrine sediment sequence, which has been dated by luminescence at its base to ~180 ka. In the upper parts of these lake deposits, Anselmetti et al. (2010) found anomalies in shear-strength measurements and deformed sediment textures, both of which were interpreted as the possible result of a temporary ice-overload around 140 ka (MIS 6).

## 3. Materials and methods

### 3.1. Seismic survey

Four multichannel seismic lines were acquired in May 2008. One line (NW-S1, 3.9 km long; location shown in Fig. 1B) runs

parallel to the main valley axis, while three shorter lines (NW-S2, S3, and S4; 1.0–1.3 km long) cross the valley in a perpendicular direction. In general, explosive sources triggered in 0.8 m deep holes were used, although, in sensitive areas, a hammer source was applied instead. Both sources resulted in a dominant frequency of 10–50 Hz. Shot spacing ranged between 3 and 5 m. 216 active channels were recorded with a sampling rate of 0.25 ms and a length of 2 s. Prior to stacking, data were cleaned, static-corrected, gained, and time-variant filtered (10/45–200 Hz). Velocity analysis was performed every 105 and 63 m for long and cross profiles, respectively. After stacking, data were deconvoluted (frequency/distance domain), and converted from time to depth using a velocity function based on the stacking velocities.

### 3.2. The core NW09

The 93.6 m long sediment core NW09 (47.50456°N, 8.380295°E, 455 m above sea level; Fig. 1B) was drilled using rotary and percussion drilling techniques c. 400 m SE of the palaeontological site and the coring locations of 1983 and 2007. The large coring diameter of 326 mm at the surface, slimming down to 145 mm at the bottom, allowed the complete recovery and optimal core quality. Directly after drilling, the core was split into 1 m-segments, packed in plastic foil and stored. These core segments were later split, their surfaces carefully prepared and then digitally photographed. One half was used for further sub-sampling and U-channel extraction, while the other half was described macroscopically, and lithotypes and stratigraphic units were defined. Smear slides (two for each 1 m-segment) were prepared to identify the major lithologic constituents.

### 3.3. Physical properties and grain-size

The prepared surface of one core half was analysed for shear-strength every ~30 cm using a manual Eijkelkamp vane-shear device. Magnetic bulk susceptibility and wet bulk density ($\gamma$-ray-based, $^{137}$Cs source) were measured with a GEOTEK Multisensor Core Logger (MSCL) using U-channels at 3 and 1 cm spacing, respectively. Grain-size of the sediments was estimated macroscopically on the split surface so that silt, sand, and gravel distribution could be established during core description. These data were quantitatively complemented with laseroptical measurements every ~20 cm using a Malvern Mastersizer (0.02–2000 μm).

### 3.4. Geochemistry

Total inorganic carbon (TIC), total organic carbon (TOC), total sulphur (TS), and total nitrogen (TN) content were determined every ~30 cm. Total carbon (TC), TS, and TN were measured using an elemental analyser (HEKAtech Euro EA, Elemental Analyser). TIC was measured using a titration coulometer (Coulometric Inc., 5011 CO2-Coulometer) and calcium-carbonate contents were calculated by multiplying TIC by 8.33. TOC was calculated by subtracting TIC from TC.

### 3.5. Palynology

372 sediment samples (2–8 cm$^3$) were taken at 2–50 cm intervals for palynological studies. From this set, 99 samples were spiked with *Lycopodium* spore tablets following Stockmarr (1971) and chemically prepared for analysis using HCl, HF, and acetolyses (Erdtmann, 1934). For some samples this process was extended using $ZnCl_2$ (2.0–2.1 cm$^{-3}$) in order to deplete the zircon detritus. Finally, the material was repeatedly rinsed with glycerol to remove the finest organic remains. For each sample, 500 pollen grains were microscopically analysed and counted at magnifications of 400–1000×. If less pollen grains were present in the sample, the entire microscope slide (24 32 mm) was analysed. Pteridophytes, aquatics, pre-Quaternay sporomorphs, and indeterminanda were excluded from the pollen sum (arboreal pollen (AP) and non arboreal pollen (NAP) = 100%) for calculation of percentages. The spores of ferns and mosses and the non-pollen palynomorphs (NPP; includes algae, fungi, mandibles of chironomids, and other remains of invertebrates) are expressed referring to the pollen sum. The stomata are presented as number of counted findings. The results are presented as a percentage pollen diagram. Local pollen-assemblage zones (LPAZ) are defined manually according to Cushing (1964, cited in Birks, 1986). Samples with a pollen sum <20 grains per slide were considered as pollen-free and are marked by a dotted line in the pollen diagram.

### 3.6. Remanent magnetisation and anisotropy of susceptibility

Directions and intensities of the natural remanent magnetisation (NRM), using U-channel material, were measured every 2 cm with a fully automated long-core 2 G-Enterprises DC-SQUID 755 SRM magnetometer with an integrated in-line triaxial alternating field (AF) demagnetiser. Demagnetisation was carried out in nine steps with AF levels from 0 to 65 mT. Directions of the characteristic remanent magnetisation (ChRM) were derived by principle component analysis (Kirschvink, 1980) of the results of successive demagnetisation steps. Measured NRM signals are integrated over 10 cm U-channel length. All U-channels were obtained without azimuthally orientation. Therefore the mean ChRM-declination value of the top of each U-channel was set to zero. For investigation of the magnetic sediment fabric, the anisotropy ellipsoid of the magnetic susceptibility (AMS) was determined. For this purpose, 124 cylindrical specimens (c. 3.4 cm$^3$) were later taken from U-channel material every 15 cm at core depths of 70–88 m. This set was measured using a Geofyzika Brno KLY-2 Kappabridge with an operating frequency of 920 Hz and a coil sensitivity of $1 \times 10^{-8}$ SI. The specimen susceptibility was measured manually in 15 different directions following the scheme of Jelínek and Kropáček (1978). These measurements are fitted to the susceptibility tensors with a least-squares method using the software ANI20BAS.

### 3.7. Luminescence dating

Sampling was restricted to consolidated sediments where it was clear that the inner parts of the core had not been exposed to light subsequent to extraction. The outer layers were removed under subdued orange light in the laboratory. All grains were treated with 32% hydrochloric acid to remove carbonates, 30% hydrogen peroxide to remove any organic component, and sodium oxalate to prevent aggregation of the grains. Polymineral fine grains, 4–11 μm, were settled in Atterberg cylinders using Stokes' law. To obtain a quartz fraction, a portion of these were immersed in 31% hydrofluorosilicic acid for one week, followed by rinsing with 32% hydrochloric acid to remove fluorides. Where an infra-red (IR) stimulated signal was present, immersion in hydrofluorosilicic acid for a further week was able to successfully remove any feldspar contamination. For eight of the 29 samples taken, it was not possible to isolate a quartz fine-grain fraction. Fine grains were settled on stainless steel discs using acetone. All measurements were made on automated Risø TL/OSL DA-20 readers, fitted with an EMI 9235QA photomultiplier tube. Stimulation was performed at 90% power, using blue (IR) LEDs for quartz (polyminerals), with the signal detected through 7.5 mm of Hoya U-340 transmission filter (410 nm interference filter and one Schott BG-39).

For each sample, 400–500 g of material was taken from the surrounding sediment for dose rate calculations, and the specific activities of U, Th and K were determined using high-resolution gamma spectrometry (cf. Preusser and Kasper, 2001). Although water content was determined using conventional oven dry method, the results were unusually varied suggesting a problem with subsequent loss of water following coring. For this reason, an averaged palaeo-water content of 30 ± 5% was applied and considered to be appropriate to such sediments.

All Equivalent Dose ($D_e$) measurements were made using a modified version of the Single Aliquot Regenerative Dose (SAR) protocol (Blair et al., 2005; Murray and Wintle, 2000). Preheat and dose-recovery tests had been conducted on samples from this site by Anselmetti et al. (2010); temperatures of 230 and 270 °C for 10 s, were applied to quartz and polymineral grains, respectively; dose-recovery tests were within 1% (10%) of unity for quartz (polymineral) grains. Unless otherwise stated, between three and five aliquots were measured for each sample and $D_e$ measurements with recycling ratios over 10% of unity were rejected. Recuperation of the luminescence signal remained below 1% (3%) for OSL (IRSL). Quartz $D_e$ values were determined using the first 0.4 s of the OSL decay curve, and subtraction of an early background calculated using 1.0–1.4 s (Ballarini et al., 2007). $D_e$ values for polymineral grains were determined using the first 10 s of the IRSL decay curve, with background subtraction calculated using the last 200 s. Both the quartz OSL and the polymineral IRSL dose response fitted well to a saturating exponential plus linear function (Fig. 2) and this was used to determine $D_e$ values.

When measuring feldspar it is important to monitor for anomalous fading, whereby the luminescence signal has been shown to decay significantly without stimulation (Aitken, 1985; Wintle, 1973), resulting in age underestimation. As the IRSL signal generated in polymineral grains is dominated by a feldspar signal, fading tests were conducted on four aliquots of this fraction from sample NWE 19. Aliquots were given a dose of 100 Gy, and this was then measured, but with increasing pauses placed between the preheat of the regenerative dose and IRSL stimulation. Fading of the laboratory-induced signal was detected and quantified by a g-value of 2.05 ± 0.80%, which can then be utilised by one of several methods (Auclair et al., 2003; Huntley and Lamonthe, 2001; Lamonthe et al., 2003), to correct the measured burial dose for fading. However, these methods rely on the assumption that the fading occurs logarithmically, and continues to do so over geological time, and should only strictly be applied to burial doses that lie on the early, linear part of the dose response curve. Additionally, it has recently been suggested that fading measured in the laboratory, albeit on a high temperature IRSL signal, may just be an artefact of the measurement procedure (Thiel et al., 2010). For these reasons, it was considered prudent to leave IRSL ages uncorrected, although it should be noted that such a correction would lead to a minimum increase in age of 20%.

Klasen et al. (2006) found that the optical bleaching characteristics of the luminescence signal from quartz and feldspar differed and so a bleaching experiment was conducted on both mineral fractions. Aliquots of samples NWE 6 and 19 were prepared and then exposed to light from a Sunlux Ambiance UV lamp, for 0, 15, 30, 45 and 60 min, prior to measurement of the $D_e$. As the sediment was waterlain prior to burial, a Schott GG495 optical filter was placed in front of the samples to simulate water and attenuate the light. Results from this experiment are illustrated in Fig. 3. Although the natural signals measured for quartz and polyminerals varied between 300 and 660 Gy, all values were reduced to <40 Gy following 30 min exposure to daylight. However, further reduction of the polymineral IRSL signal then slowed, and after 1 h of exposure this fraction still retained ~15 Gy more signal than the quartz which was reduced to <6 Gy.

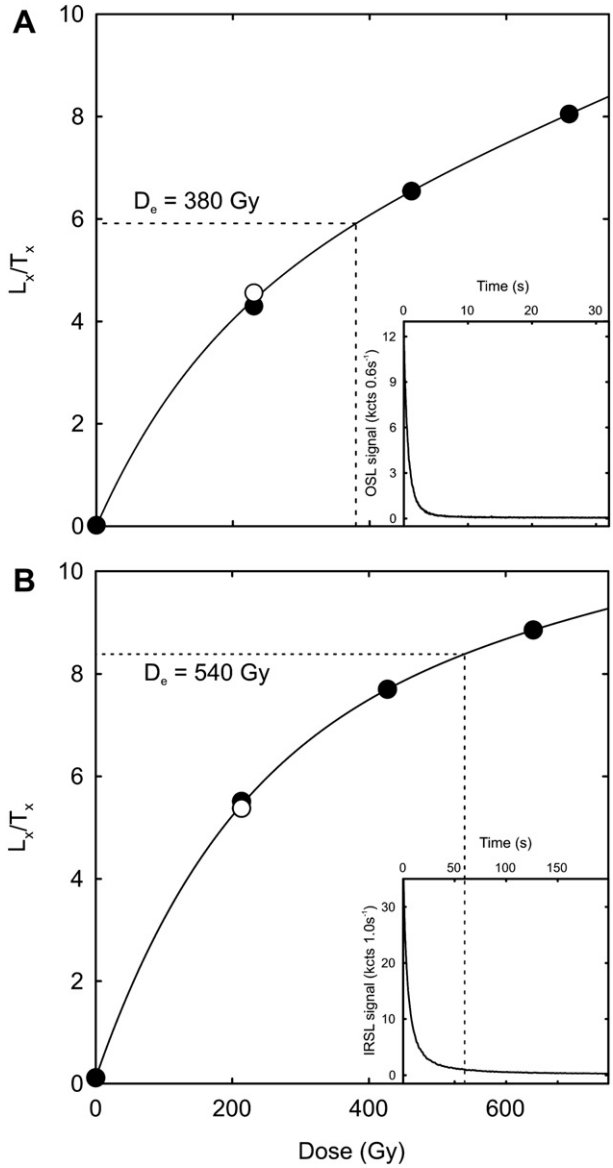


**Fig. 2.** The sensitivity corrected dose response for quartz OSL (A) and polymineral IRSL (B), for sample NWE 7 (60 m depth). Both fit best to a saturating exponential plus linear function. The dashed line indicates the $D_e$ value, and the recycle point is indicated by the empty circle. Inset for both figures is the natural decay curve for each sample.

## 4. Results, data evaluation and interpretation

### 4.1. Seismic data interpretation

The recorded and processed seismic data recognised four seismic units (Fig. 4A). The lowermost Unit 1 shows low amplitudes (almost transparent) with chaotic reflections. Unit 2 above displays high-amplitude hummocky reflections, Unit 3 is characterised by sub-parallel medium-amplitude reflections that show onlaps onto Unit 2. Seismic Unit 4 is almost transparent and shows no continuous reflections.

A number of previous drillings (Anselmetti et al., 2010; Graf and Müller, 1999; Schlüchter, 1988a) and an unpublished bedrock depth map of the investigated area were available to support the interpretation of the acquired seismic lines and to interpret in more detail the lithologic content of the seismic units (Fig. 4B). Based on these additional data, Unit 1 is identified as bedrock (Lower

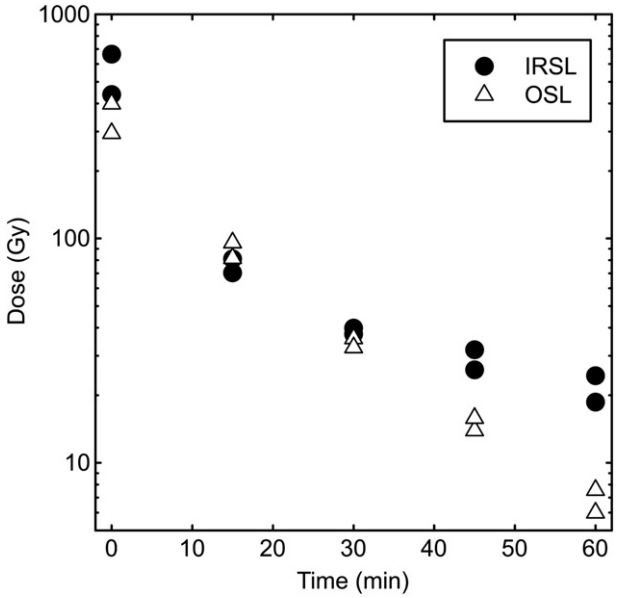


**Fig. 3.** Bleaching experiment conducted on the polymineral (IRSL) and quartz (OSL) fraction of samples NWE 6 and NWE 19. Aliquots were placed under a Schott GG495 optical filter to simulate the attenuating effect of water on daylight and exposed to light from a Sunlux Ambiance UV lamp for 0, 15, 30, 45, and 60 min, prior to measurement of the $D_e$. Each datapoint is the average of five aliquots.

Freshwater Molasse, alternation of clay, marl, and sandstone). Unit 2 is interpreted as coarse unconsolidated sediments as generally found at the base of basin fillings, and reflects a heterogeneous sequence of till and subglacial gravel. Unit 3 consists of mainly sandy, probably cross-bedded sediments that most likely represent deposition by a delta. Unit 4 represents fine-grained lake deposits. Fig. 4B shows further units that could not be identified in the seismic survey but are clearly evident from core data, e.g. the peat deposits in the upper part of the lake sediments of Unit 4.

### 4.2. Physical properties and lithology

The evaluation of the physical properties and geochemical composition of core NW09 shows distinct variations that allow the definition of well characterised lithostratigraphic units (Fig. 5), with the varying lithotypes presented in the online supplement.

The deepest drilled **Unit A** (93.60–89.50 m) of NW09 consists of grey to greenish weakly consolidated sands and loose silts with a bulk density of 1.7–2.1 g cm$^{-3}$. Between 92.80–92.00 m, the silts show a well-developed stratification with unconsolidated sands. $CaCO_3$ content is typically in the range of 7–26 wt% (average of c. 18 wt%). This unit contains no significant amounts of organic carbon, nitrogen or sulphur. Shear-strength displays a prominent increase at 90.65 m, indicating significant overconsolidation of the uppermost 1.15 m. Smear slide studies show sub-angular to sub-rounded quartz and feldspar grains as main components, as well as a large mica portion. Heavy minerals comprise mainly epidote and garnet. Noteworthy are two brown to reddish horizontal horizons at 90.60–90.70 m and 90.20–90.16 m composed of clayey silt.

The unconformably overlying **Unit B** (89.50–84.60 m) generally consists of grey to brown sandy silts with uniformly distributed mm-sized dropstones. It is vaguely laminated and shows distinct shear and deformation structures in parts. Occasionally this succession is interrupted by poorly sorted coarse beds with a silt matrix and clast-sizes of ≤7 cm. The clast material comprises

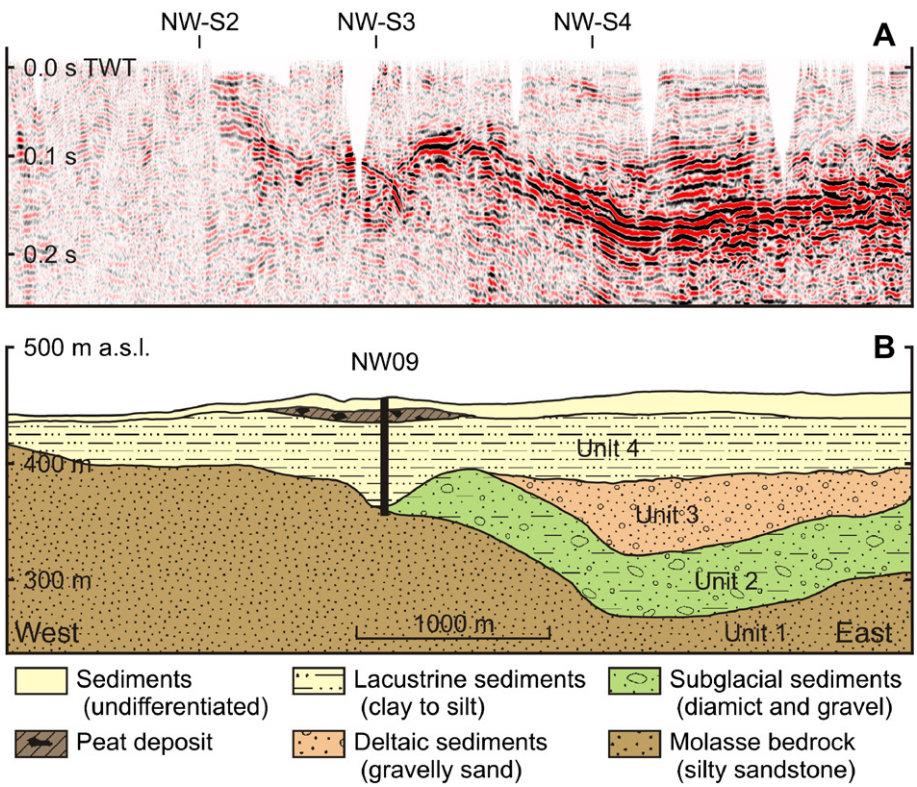


**Fig. 4.** A) Uninterpreted seismic line NW-S1 (for location see Fig. 1B). *y*-axis is two-way traveltime (TWT) in seconds. (B) Interpretation of seismic line NW-S1 based on seismic data and other drill cores near Niederweningen with indication of drill site of core NW09 and identified seismic units (for details see Section 4.1). Vertical exaggeration is ~5×. The seismic section was converted to depth in metres using a velocity function based on the stacking velocities.

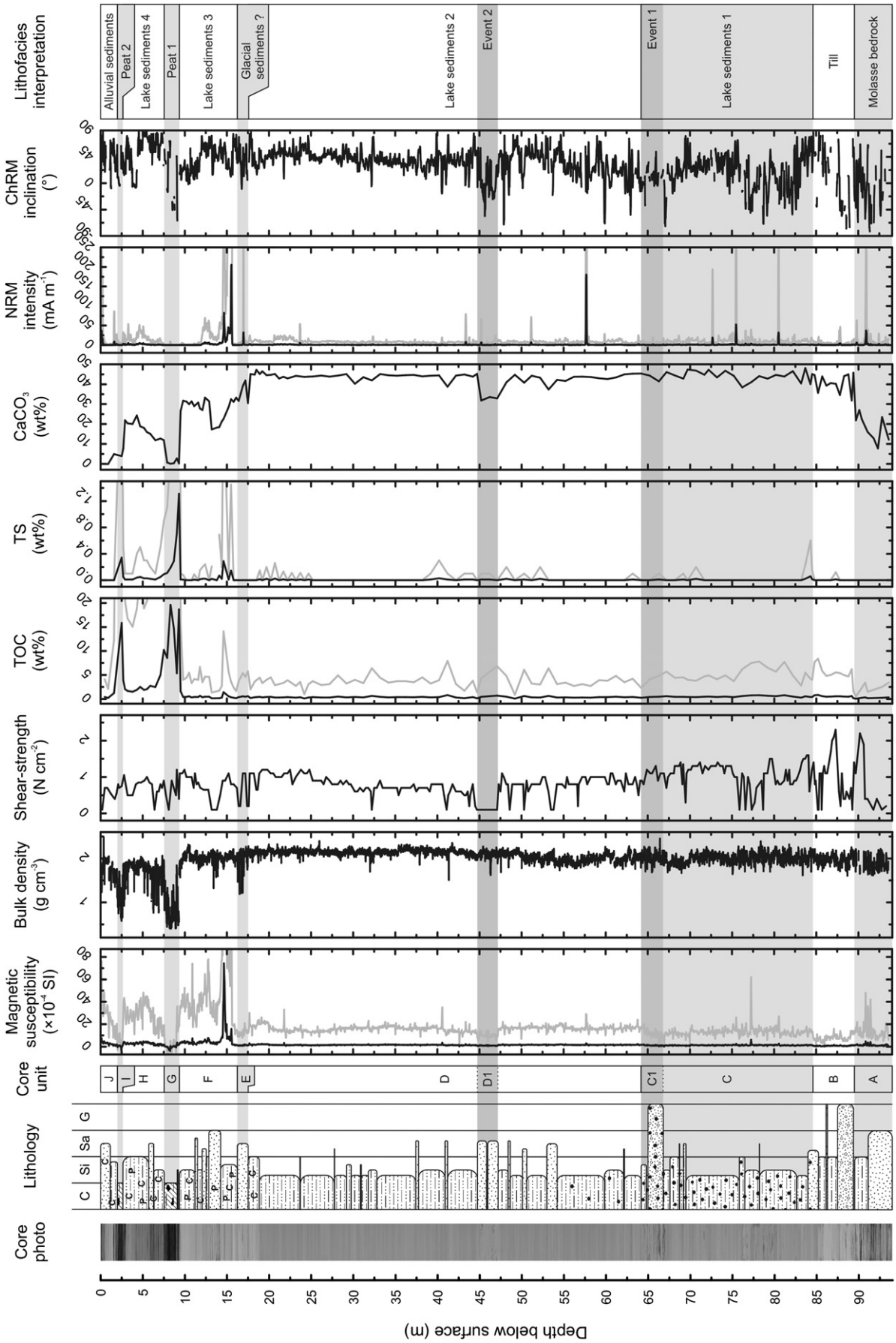


**Fig. 5.** Main data overview of the core NW09 with core photo, schematic lithology log (C/Si/Sa/G codes clay, silt, sand, and gravel; black dots represent ice rafted debris; P is pyrite-rich horizons; C is carbonate-rich concretions; crosshatch represents peat), bulk density, shear-strength value, total organic carbon (TOC) and total sulphur (TS) content, organic carbon to nitrogen ratio (C/N), and carbonate ($CaCO_3$) content. Grey line in TOC, TS, NRM, and magnetic-susceptibility columns is measurement ×10. Right column shows lithofacies interpretation of the core units.

mostly dark grey to black limestone and siliceous limestone (Helvetic nappes), some conglomerate and sandstone (Subalpine Molasse), quartzite (Austroalpine nappes), few crystalline basement rocks (Vorder- and Hinterrhein area), and a single clast of red conglomerate (Permian Verrucano of the Helvetic nappes). Both, the fine-grained and the diamictic deposits are characterised by a significant increase in $CaCO_3$ content to ~41 wt% and marginally increased TOC content. While the bulk density is constant and comparable to Unit A, this unit includes an overconsolidated section (87.40–85.40 m) with a prominent peak in the measured shear strength of 2.3 N $cm^{-2}$. Magnetic susceptibility is slightly increased to $\sim 0.80 \times 10^{-4}$ SI. The mineral spectrum is composed of quartz, feldspar, calcite, a few micas, zircon and accessory garnet.

Unit B is overlain by 20 m of dark grey silty clay to clayey silt (Unit C; 84.60–64.20 m). A characteristic mottled lamination in mm to cm-scale is clearly visible (lighter/darker grey shades), as well as sporadic undeformed parts. The sequence is further characterised by periodically occurring angular to sub-angular dropstones with a size of a few mm to some cm and occasionally (fine) sand lenses. Bulk density fluctuates around 2.0 g $cm^{-3}$, TOC is still very low (0.5 wt%), and $CaCO_3$ content increases slightly to ~44.2 wt%. Shear-strength data shows fluctuates around 1.0 N $cm^{-2}$, which is most probably caused by localised clay bands and sand lenses. Slightly increased values of ~1.25 N $cm^{-2}$ are observed from 75.00–68.20 m. Quartz, feldspar, calcite, with some mica, are the most abundant minerals, while the heavy minerals are characterised by some garnet and rutile grains. A striking increase in dropstone quantity and size (up to 20 cm) occurs at the top of this unit (**Sub-unit C1**; 66.80–64.20 m). Although dropstones are frequent in the lowermost 80 cm of this C1 layer, a fine lamination of the matrix is still noticeable. Physical properties and geochemical data are similar to the main part of Unit C.

Overlying **Unit D** from 64.20 to 17.60 m shows similarities to Unit C although the dropstones are smaller (<2 mm), occur less frequently and are not present above a depth of 56.70 m, except for a single occurrence at 17.88 m. The unit also comprises grey laminated clayey silt to silty clay and occasional pure clay beds, as well as well discontinous sand lenses. A mottled lamination results from minor grain-size differences (darker laminations contain more clay) and its thickness varies at 3–4 mm in the more distinct lower part, to 1–2 mm in the upper part. TOC averages ~0.4 wt% and $CaCO_3$ ~43.2 wt%. Bulk density shows typical variations around 2.1 g $cm^{-3}$. The negative peak of 1.5 g $cm^{-3}$ at 41.35 m is related to an incompletely filled U-channel. Shear strength values vary around 0.79 N $cm^{-2}$ and then increase up-core to 1.20 N $cm^{-2}$ starting around 30 m, with a sudden drop back to lower values at a depth of 18.83 m. This deterioration is associated with changes in the sediment colour (to brownish) and grain-size (to silt/fine sand interbedding). Above a depth of 17.90 m, white carbonate-rich concretions (spheroids) in sub-mm size can occasionally be observed. Magnetic susceptibility averages $1.58 \times 10^{-4}$ SI and is slightly higher than Unit C. Mineral composition shows no significant changes. The uniform sediment composition is interrupted by a second prominent layer at a depth of 47.20–44.75 m (**Sub-unit D1**). Here, the weakly silty fine/middle sand shows a reduced $CaCO_3$ content of ~36 wt% and very low shear-strength values of 0.1 N $cm^{-2}$. Magnetic susceptibility is also lower ($\sim 0.99 \times 10^{-4}$ SI). The vague lamination is deformed as is the surrounding fine-grained unit.

**Unit E** (17.60–16.25 m) starts with a conspicuous drop in $CaCO_3$ concentration below 40 wt%. This unit is made up of silt/sand alternations in cm to dm scale. Occasionally, larger single clasts (some mm up to 4 cm in size) are embedded in a finer-grained matrix. The largest clasts comprise whitish limestone (at 17.20 m, 16.49 m, and 16.39 m) and weakly consolidated sandstone (16.50 m). Possible source rocks are Late Jurassic limestone and Palaeogene–Neogene molasse sandstone beds from the northern Lägern flank. TOC concentrations for the entire unit remain low. Bulk density shows strong local fluctuations between ~1.2–2.3 g $cm^{-3}$, especially at 17.00–16.64 m and 16.50 m, due to inappropriately filled U-channels caused by the grain-size variations. This is also the case for the variation in the shear-strength measurement, where sand layers produce negative peaks.

Overlying **Unit F** (16.25–9.35 m) begins as a grey-greenish weakly laminated clayey silt, changing to alternating silt and sand (grey to greenish and occasionally rock fragments (<2 mm)), and finally to fine laminated grey bluish silt. The upper silt section shows local brownish spots up to cm scale, identified as iron-rich clay pockets. Commonly occurring black framboidal pyrite grains and carbonate-rich concretions both <1 mm in size, are prominent in this unit. Positive peaks in the organic carbon and sulphur concentrations, as well as the magnetic susceptibility record are coincident with the highest pyrite abundance around 15.60–14.00 m. The $CaCO_3$ content drops below 20 wt% in a largely sandy section (~14.10–13.20 m), and levels off at 30 wt% in the overlying silt. Bulk density averages 2.0 g $cm^{-3}$, with a short excursion to lower values at about 14.00–13.40 m. Unit F incorporates the first occurrence of macroscopically visible plant remains at a depth of 14.55 m, often enriched in very thin layers. Smaller wood or root fragments appear around 10.80 m. Bulk density values steadily increase in the uppermost 30 cm of Unit F as the amount of organic remains increase.

**Unit G** (9.35–7.55) begins with an abrupt change to a 10 cm thick well-developed brown blackish pure peat horizon, followed by alternating peat and organic-rich clay and silt, and a second pure peat horizon at 8.25–8.00 m. This switch to increased organic matter is associated with decreased bulk density and $CaCO_3$ minima, as well as in pronounced positive peaks in TOC (18.7 and 19.6 wt%) and TS (1.3 wt%). The magnetic susceptibility shows characteristic negative values for the two pure diamagnetic peat horizons and decreased values ($\sim 0.5 \times 10^{-4}$ SI) in the organic-rich silt.

The clastic sediment of **Unit H** (7.55–2.65 m) is in the lower part made up of organic-rich silty sand, with the occurrence of some washed in peat patches. At a depth of ~5.80 m the composition changes to slightly sandy silt and then to slate blue weakly laminated clayey silt at a depth of ~4.50 m. The uppermost 0.65 m returns to bluish clayey silt, containing lumps of humic silt. An irregular pattern of rust-coloured patches is noticeable within the finer-grained portions of Unit H. TOC and TS concentrations level off around 2.2 and 0.3 wt%, respectively. $CaCO_3$ content gradually increases again to values around 20 wt%. Bulk density and shear-strength show larger variations. The bulk density averages 1.35 g $cm^{-3}$ in the organic-rich lower part then increases to ~1.82 g $cm^{-3}$, and finally decreases again to ~1.54 g $cm^{-3}$. Variations in the shear-strength values of 0.10–1.05 N $cm^{-2}$ are most probably caused by the inhomogeneous grain-size distribution. Magnetic susceptibility steadily increases to $4.8 \times 10^{-4}$ SI and then averages $2.9 \times 10^{-4}$ SI.

**Unit I** (2.65–2.00 m) displays a dark brown peat deposit intercalated with silt slices at its very top. $CaCO_3$ concentration averages 3.9 wt%. Bulk density and magnetic susceptibility show, as one would be expect for biogenic sediments, decreased values around 1.1 g $cm^{-3}$ and $0.15 \times 10^{-4}$ SI. TOC and TS show significant positive peaks up to 15.87 and 0.35 wt%, respectively.

The topmost **Unit J** (2.00–0.00 m) starts with humus-rich grey to slate blue clayey silt, changes into brown sandy silt to silty sand and finally, in a depth of ~0.7 m, into the recent soil. Carbonate content is ~4.9 wt% in silty parts and zero in the soil. TOC shows a massive decrease to values around 0.8 wt%, while magnetic

susceptibility and bulk density increase to $2.3 \times 10^{-4}$ SI and 1.87 g $cm^{-3}$, respectively.

### 4.3. Interpretation of lithostratigraphic units

Unit A (93.60–89.50 m) is interpreted as typical Lower Freshwater Molasse (Oligocene/Miocene), which forms the bedrock of the drilled overdeepened trough. This interpretation is supported by the observed characteristic sediment colour, the low carbonate content and typical high epidote and mica abundances (Bitterli-Dreher et al., 2007). Both observed reddish horizontal layers are interpreted as relict palaeosols, though no clear indication for soil formation can be confirmed. It is unclear if the observed unconsolidation results from the drilling operations or if it was caused by physical weathering under permafrost conditions just prior to deposition of the overlying till unit (see below). The alternation of silt and diamict containing Unit B (89.50–84.60 m) suggests deposition as subaqueous diamicton (waterlain till). Additionally, the overconsolidated layer suggests temporary ice-overload and consequently subglacial conditions. The clast lithologies are characteristic of the Walensee Glacier (Hantke, 1978).

The fine-grained Unit C (84.60–64.20 m) with its dropstones is interpreted as proglacial lake sediments containing typical ice rafted debris, originating from drifting icebergs. The observed $CaCO_3$ contents of ~45 wt% are comparable to the reported 45–50 wt% in glacial sediments studied by Jenny and de Quervain (1961) in the Walensee area. This points to a mainly allochthonous carbonate input into the Wehntal derived by the Walensee Glacier. Sub-unit C1 (66.80–64.20 m), with its high dropstone abundance at the end of the proglacial lake sequence, is believed to represent a massive ice berg calving event, such as an ice-front collapse during the retreat of the Walensee Glacier.

Unit D (64.20–17.60 m) is mostly fine grained with some sandy intercalations and shows only a marginal dropstone content in its lower part. Unit D is therefore interpreted as detrital distal lake sediments (finer-grained) with occasional shifts to a more proximal position (coarser grained). The sandy deposits may also result from high-energy events that temporarily increased the input of suspension load (e.g. meltwater outbursts or river floods) into a usually calm lacustrine environment. Extended transport distance by density-controlled underflow currents may further contribute to a more distal sedimentation of coarser grained detritus. The sand dominated sub-unit D1 (47.20–44.75 m) is interpreted to represent either a very pronounced high-energy event, or a possible subaqueous delta-front collapse producing a grain-flow deposit (Cohen, 2003). The reduced $CaCO_3$ contents within this coarse event layer most probably reflect a grain-size effect, as the detrital carbonate typically occurs in the finer silt fraction. The very low TOC abundance and the lack of organic remains such as snail, diatom, and ostracod shells or chironomid jaws, indicates reduced primary production in the water body. The presence of laminations further indicates a lack of bioturbation and hence no active benthos. Following Collinson et al. (2006), the whitish carbonate-rich concretions, starting at a depth of 17.90 m, are probably of post-sedimentary origin and formed during an early stage of sediment diagenesis. These precipitates are often formed in response to bacterial sulphate reduction which itself requires some amount of organic material. At a depth of ~18.8 m, the sediments begin to coarsen and change to brownish colours, due to continuing infilling or lowering of the outflow level.

The decreasing $CaCO_3$ content at the beginning of Unit E (17.60–16.25 m) is interpreted as an indication for dramatic changes in the Wehntal's catchment area. As shown above, the Walensee Glacier is most probably the major carbonate source, and so the $CaCO_3$ decrease may document a melting back of the glacier behind the sill near Niederglatt or Hombrechtikon (see Fig. 1A), causing greatly reduced discharge into the Wehntal or Glatt Valley. A larger mean grain-size (up to sand) also indicates a lasting lake level recession. Interpretation of the observed isolated matrix-embedded single clasts is, however, ambiguous. The clasts might represent melt-out debris from icebergs (dropstones), or they may represent lateral slope debris, fallen onto a frozen lake and then rafted to a more distal position. Both transport mechanisms will result in the observed facies but will have divergent environmental implications. Considering the clast lithologies and the striking $CaCO_3$ decrease, ice floe transportation seems more likely.

Unit F (16.25–9.35 m) shows fine-grained lacustrine sediments with intermittent interbedded sand. Commonly occurring pyrite grains as well as, carbonate concretions suggest early diagenetic microbial decomposition of organic matter under anaerobic conditions (Berner, 1984; Chowdhury and Noble, 1996; Peckmann et al., 2001; Psenner, 1983). A later post-sedimentary pyrite formation, however, is also possible. Calvert et al. (1996) describe pyrite freshwater-precipitates that were formed from downward diffusion of sulphate and/or sulphide from overlying organic-rich strata. This process would imply that the pyrite depth reflects the recent position of a sulphate (sulphide) diffusion horizon and not the palaeoenvironmental conditions at the time of, or close to sediment accumulation. The first occurrence of macroscopic plant remains documents a climate improvement and, in combination with coarser grained sediments, a progressive shallowing of the lake.

This silting-up trend culminates in Unit G (9.35–7.55 m) with the growth of pure peat in a typical wetland environment. The organic-rich clay and silt suggests that this swamp phase was affected by short-term re-flooding. These mainly clastic accumulations are then again overlain by a pure peat deposit. The flooding does not necessarily require the formation of a small lake or pond, and a braided channel network of the Palaeo-Surb River is also a reasonable possibility. Based on the stratigraphic position of Unit G, the peat layers are similar to a peat horizon drilled in NW07 (Anselmetti et al., 2010) and KB 2–83 (Welten, 1988).

Unit H (7.55–2.65 m) consists of organic-rich silty sand with scattered, probably reworked peat patches and is therefore interpreted as a renewed lake phase under moderate climate conditions. A re-flooding of the Wehntal requires temporary changes in the valley's outlet configuration, e.g. dam-like structures. A potential location for this temporary blockade might be found in the gorge-shaped western valley outlet, although field observations ensured no evidence.

The dark brown peat of Unit I (2.65–2.00 m), with its overlying silt patches bears witness to a renewed silting-up, and the formation of marsh land. Its profile depth suggests correlation to the well studied 'mammoth peat' (c.f. Furrer et al., 2007 and chapter 2). The incorporated silt lumps document deformation and/or reworking of the upper peat section. This feature is documented elsewhere and most probably results from cryoturbation processes (Furrer et al., 2007; Schlüchter, 1988a, 1994).

The silt and sand of the topmost Unit J (2.00–0.00 m) represent fine alluvial sediments, probably deposited in shoaling pond. An upward coarsening of the grain-size might represent the influence of the Singelenbach alluvial fan, with the absence of gravel suggesting a more distal position to this debris fan. The uppermost silty sand shows a typical brown earth-podzol development.

### 4.4. Pollen record

The pollen content of NW09 shows good to excellent pollen preservation and allows for the definition of five main local pollen-assemblage zones, including some sub-zones. A reduced pollen diagram is shown in Fig. 6.

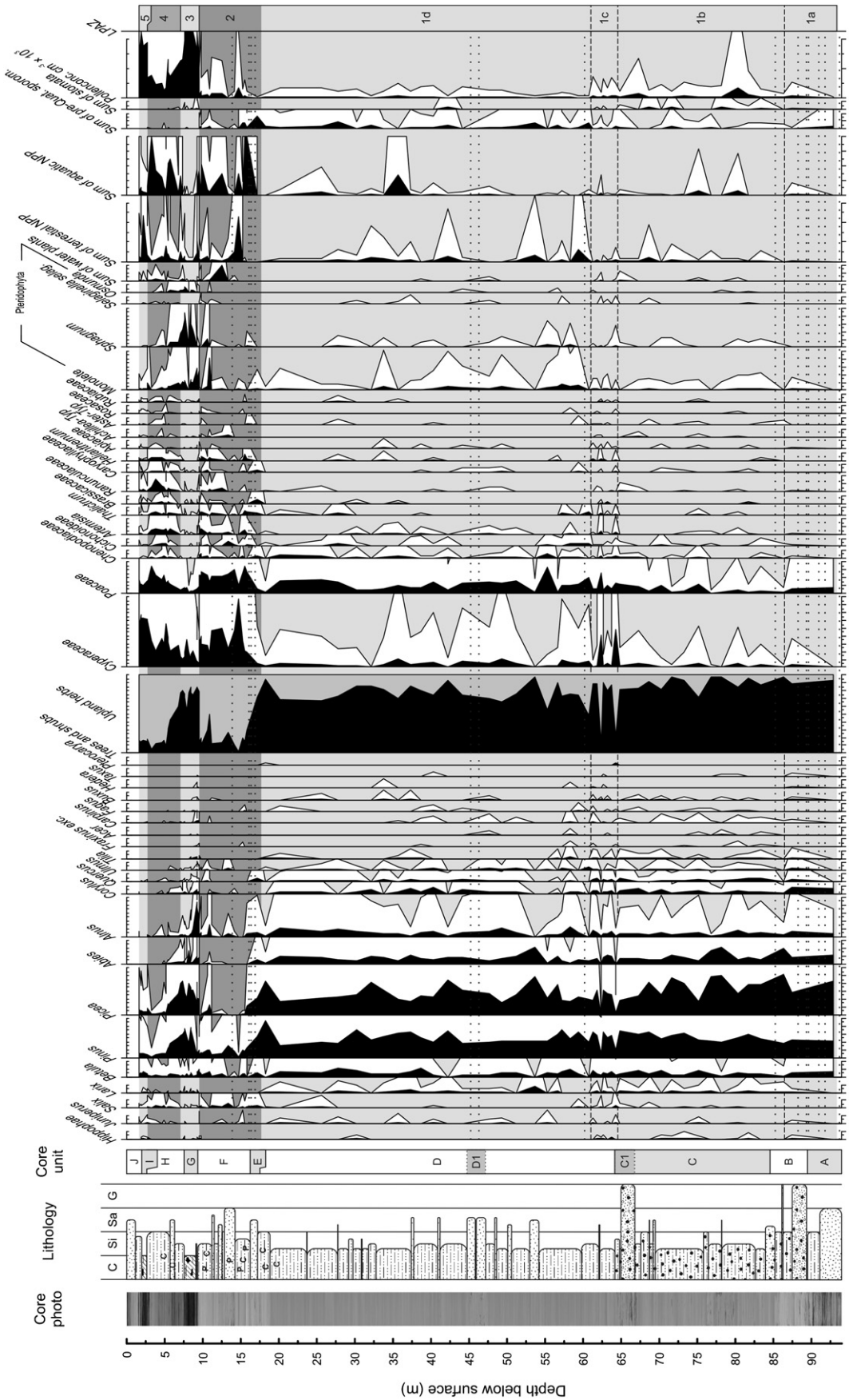


**Fig. 6.** Reduced pollen diagram of NW09. Samples with a pollen content of less than 15 grains per preparation are not included and shown as dotted horizontal lines. White areas represent exaggeration ×10 of pollen curves. LPAZ local pollen-assemblage zone.

**LPAZ 1** (93.60–17.60 m, 55 analysed samples) is characterised by a mixture of mesophilic AP (dominated by *Picea* < 50%, *Abies*, *Alnus*, and *Corylus*, accompanied by *Quercus*, *Ulmus*, *Tilia*, *Fraxinus*, *Carpinus*, *Hedera*, *Buxus*, *Taxus*, *Fagus* and the mesophilic fern *Osmunda*) and cold resistent trees (*Pinus* < 30%, *Betula* ± 10%, *Juniperus*, *Hippophae* ecc.) with heliophile herbs (e.g. *Artemisia*, *Helianthemum*, Chenopodiaceae, Apiaceae, *Thalictrum*, *Anthericum*, *Gypsophila*). Pteridophyta occur as monolet spores, *Sphagnum*, *Osmunda*, *Pteridium*, and *Selaginella selaginoides*. Water plants (e.g. *Myriophyllum*, *Potamogeton*) and other water organisms (e.g. Algae, Acari, Chironomidae, Neorhaptocoela-flatworms) are rare. LPAZ 1 is further characterised by a constant presence of pre-Quaternary sporomorphs, such as old forms of Pinaceae, *Pterocarya*; trilet spores, Dinoflagellatae and Foraminiferae and different unknown pollen types. It shows low to very low pollen concentrations, varying between 0 and 16,700 grains $cm^{-3}$, but exceeding 2500 grains $cm^{-3}$ in a few samples only. Sub-zone **LPAZ 1a** (93.60–86.50 m) is defined by its extremely low pollen concentration. Six of the eight samples are pollen-free, with the remaining samples yielding pollen concentrations of only 144 and 2600 grains $cm^{-3}$. The only slightly varying pollen curves in the following ~69 m of lacustrine sediment including **LPAZ 1b** (86.50–64.50 m, 14 samples) and **LPAZ 1d** (61.00–17.60 m, 26 samples) are interrupted by a period of high variability in the pollen flora (**LPAZ 1c**, 64.50–61.00 m, 7 samples). Here, the AP content drops twice from 80 to 20, and then to 10%. Thermophile and cold resistant tree species fluctuate in the same way. The herb-pollen spectrum consists mainly of heliophytes such as *Artemisia*, *Helianthemum*, Chenopodiaceae, *Thalictrum*, Apiaceae, *Anthericum*, *Gypsophila*, etc. Water organisms are rare. The pre-Quaternary flora is given by *Pterocarya*. Pollen concentration is 970–3400 grains $cm^{-3}$ and averages 2500 grains $cm^{-3}$.

**LPAZ 2** (17.60–9.37 m, 19 samples) shows very heterogeneous pollen-concentration distribution (52–63,200 grains $cm^{-3}$) with a clear increase towards the top of the LPAZ. The lower part (17.60–15.80 m) is almost pollen-free. *Pinus*, *Betula* and *Salix* are the dominant trees. The NAP flora reflects well-developed alpine meadows dominated by Cyperaceae and Poaceae. The aquatic organisms are represented by Chironomidae, flatworms (Neorhabdocoela), Acari, algae (*Botryococcus*, *Pediastrum*, and G 128), *Sparganium*, *Potamogeton*, *Myriophyllum*, and *Menyanthes*. Perforation plates can also be found. Pre-Quaternary sporomorphs do not exceed 2%.

*Picea* and *Pinus* dominate in **LPAZ 3** (9.35–7.00 m, 9 samples). *Alnus* (35–40%) and *Abies*, *Corylus*, *Quercus*, *Ulmus*, and *Carpinus* show a peak abundance in the lower part of this zone, accompanied by *Tilia*, *Acer*, *Fraxinus*, *Buxus*, *Fagus*, *Hedera*, and *Taxus*. *Hippophaë*, *Salix* and *Larix* occur sporadic. Herbs are species-rich, but show generally low abundances. *Sphagnum*, *Osmunda* and *Pteridium* show a regular presence, whereas *Lycopodium annotinum* only occurs occasionally. Aquatic organisms are rare. Special remains include perforation plates, stomata of *Abies*, *Picea* and *Pinus*. Pollen concentration varies between 64,000–320,000 grains $cm^{-3}$.

In **LPAZ 4** (7.00–2.65 m, 10 samples) AP gradually decreases to <20% and mesophile pollen types disappear except for *Picea*, and *Juniperus*, *Salix*, and *Larix* increase. NAP is dominated by Cyperaceae, Poaceae, and Ranunculaceae together with heliophile types as *Helianthemum*, *Thalictrum*, Brassicaceae. Aquatic organisms are represented by *Potamogeton*, *Myriophyllum*, *Ceratophyllum*, *Botryococcus*, *Pediastrum*, G 128, *Spirogyra*, flatworms, Chironomidae, Acari and other invertebrate remains. Pre-Quaternary sporomorphs are rare. Pollen concentration varies from ~14,000–64,000 grains $cm^{-3}$.

AP values of **LPAZ 5** (2.65–1.45 m, 6 samples) are <20% with *Betula*, *Pinus*, *Picea*, *Salix*, *Juniperus*, *Larix*, and *Hippophaë*. Thermophile species are absent except for single findings of *Quercus*, and *Carpinus*. Cyperaceae (60%) are the dominant NAP. Other herbs are frequent but mostly below 1% abundance. Ferns and moss spores are rare. *Gaeumannomyces* spores reflect the presences of the Cyperaceae. Pollen concentration totals ~88,000–110,000 grains $cm^{-3}$.

### 4.5. Interpretation of the pollen record

LPAZ 1 comprises molasse (Unit A), till (Unit B), and the lake sediments of Units C and D, which are interpreted to reflect ice distal but still cold environmental conditions (see Section 4.2). This interpretation is supported by i) the low productivity in the lake as inferred from the rare occurrence of water organisms, and, ii) the low but regular occurrence of cold-adapted pollen types. In contrast to this, are up to 70% mesophile trees, reflecting a more-or-less closed temperate forest. However, the concentration of pollen in the lake sediments is much too low to represent temperate forest vegetation and can be only inadequately explained by a high sedimentation rate. Characteristic for LPAZ 1 is the presence of pre-Quaternary sporomorphs, sometimes reaching >10%. These are interpreted to indicate a substantial amount of allochtonous sediment input. Similar mixed pollen assemblages have been found in other palynological investigations of pre-Holocene lake deposits in the Swiss Midlands (e.g. Küttel, 1989; Welten, 1982, 1988). Pollen concentrations have rarely been considered in these studies and only occasional has reworking of pre-Quaternary pollen been mentioned. The discrepancy within the pollen spectra was first discussed by Sidler (1988), who suggested the following four criteria to identify reworked pollen: i) mixture of temperate and cold-adapted pollen type, ii) no observable or reasonable evolution in vegetation over a long sedimentary unit, iii) too low pollen concentration for temperate lake deposits, and iv) frequent presence of pre-Quaternary sporomorpha. All these criteria apply for the LPAZ 1 and, additionally, the amount of NPP, in particular water organisms, is much too low for temperate environmental conditions. Based on these arguments the main pollen content of LPAZ 1 is interpreted as being reworked from the deposits of an older warm period. As discussed previously, such reworking is mainly associated with glacial conditions (cf. Drescher-Schneider, 2000; Pini et al., 2009; Sidler, 1988), and as a consequence, the occurrence of temperate pollen does not indicate warm-phase conditions.

With the exception of one sample (10.90 m), reworked pollen is almost absent in LPAZ 2. The pollen spectrum represents a well-developed Alpine meadow with few trees, typical for the initial phase of Late Glacial reforestation. The ecological conditions in the lake allow for the development of a differentiated flora and fauna, also typical for Late Glacial environments.

LPAZ 3 reveals a distinct evolution in the pollen record: the peak of *Alnus* at the beginning of the pollen zone is related to peaty material with a high content of degraded wood remains, associated with maximal values in *Alnus* cribriform plates. It is expected that this part of the sequence corresponds to alder carr that developed from a *Sphagnum*-Cyperaceae mire. Contemporarily recognisable is a minor input of mesophile tree from a mixed forest with *Picea* and *Abies* that is later substituted by a forest with *Picea* and *Pinus*. This pollen spectrum either represents vegetation conditions during the initial part of cooling during an interglacial or the climatically optimal phase of an interstadial. The presence of *Buxus*, *Hedera*, *Taxus*, and *Carpinus* together with the high amounts of *Abies* imply correlation with an interglacial, in this case most likely the Eemian. The high amount of *Alnus* pollen should not be used for correlation as they most likely reflect the local development of an alder carr. Similar observations have been made at sites such as Beerenmösli (Wegmüller, 1992), Füramoos (Müller, 2001) and Wurzach (Grüger and Schreiner, 1993). However, the presence of *Osmunda*, which is absent in all references sites (Drescher-Schneider, 2000; Grüger,

1979), but is present during the second Early Würmian interstadial (Odderade or Ufhusen in Switzerland) argues against a correlation with the Eemian. If this feature is characteristic for the Swiss Midlands, interpretation still remains ambiguous, as this particular pollen has not been observed at the Odderade (Ufhusen) reference site of Gondiswil (Wegmüller, 1992). As a consequence, correlation of the peat with either the Eemian or the second Early Würmian interstadial remains open.

The growth of aquatic elements within LPAZ 4 is interpreted as mounting waterlogging influence, which finally culminates in complete re-flooding of the site. At the same time, herb diversity and abundance increases, while the tree density lowers. Such changes typically reflect a broader deforestation and some removal of the vegetation cover. This is further documented by the presence of Glomus and the input of allochthonous material (low percentage of pre-Quaternary sporomorphs), and is interpreted as a climatic deterioration to stadial conditions combined with an increase in precipitation.

LPAZ 5 indicates a lowering of the water table, leading to the development of a very wet Cyperaceae/moss peat. A rise in temperature permits the spread of *Betula*, *Pinus*, and *Picea*, but not that of open woodland, which however is seen in the stratigraphically similar 'mammoth peat' deposit (cf. Drescher-Schneider et al., 2007).

### 4.6. Magnetic studies

The variations in the NRM intensity are similar to those in the bulk magnetic susceptibility, and suggest that the magnetisation is primarily controlled by the concentration of magnetic particles and thus reflects the heterogeneous composition of the sediments (Fig. 5). The lowest intensities ($\sim$0.01–0.04 mA m$^{-1}$) were obtained from organic-rich layers (peat), and the highest NRM intensities ($\sim$200–120 mA m$^{-1}$) were recorded in a short section showing significant pyrite precipitation (see Section 4.2). These higher values indicate a distinct change in either detrital composition (more

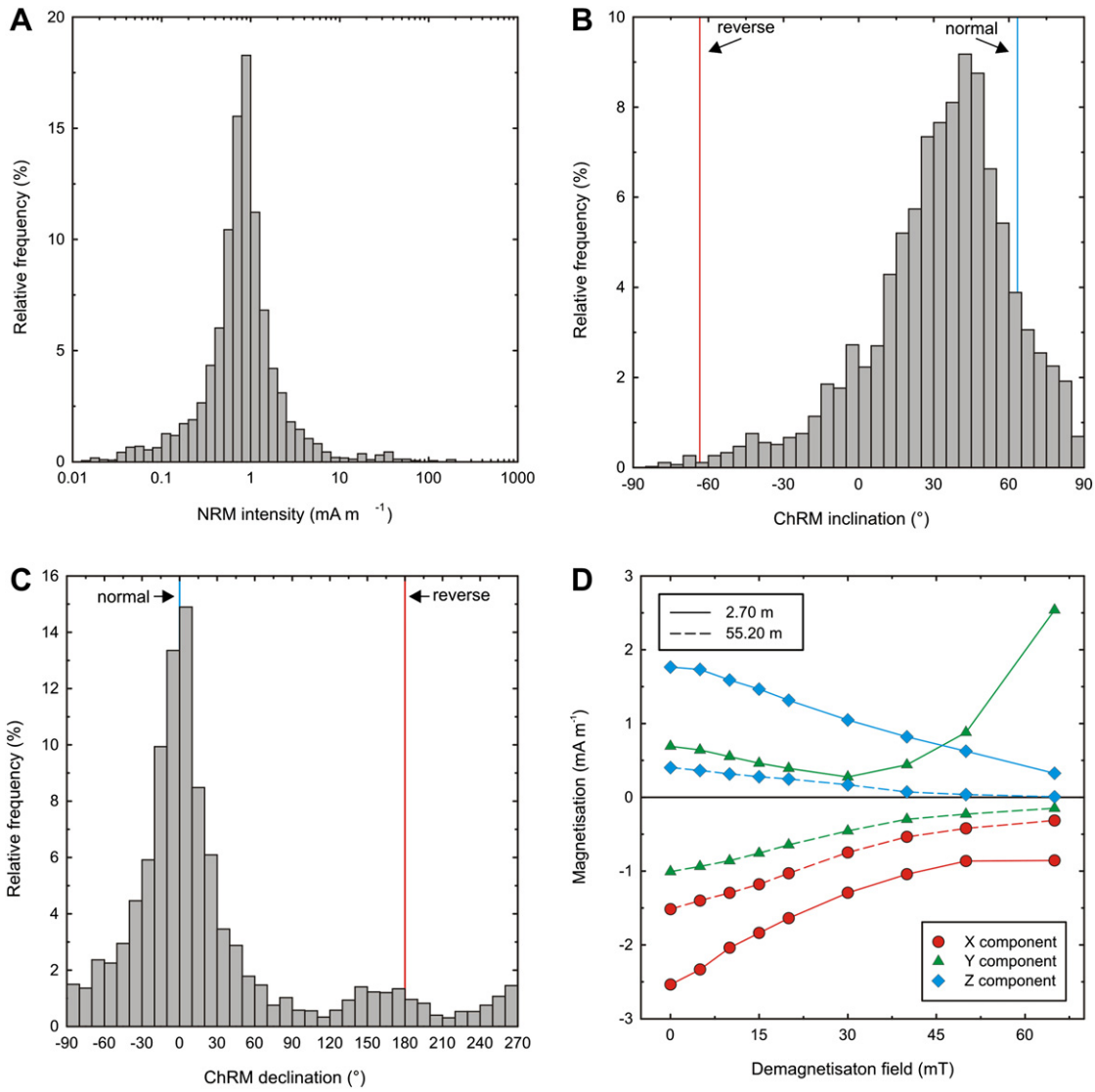


**Fig. 7.** Remanent magnetisation characteristics of core NW09. Frequency distribution of (A) natural remanent magnetisation (NRM) intensity, (B) characteristic remanent magnetisation (ChRM) inclination, and (C) ChRM declination directions. (D) Demagnetisation curves of Cartesian components (*X* circle, *Y* triangle, *Z* diamond) of two samples showing normal NRM decay during AF demagnetisation for 55.20 m sampling depth (dashed line) and beginning of acquisition of new magnetisation at about 30 mT for 2.70 m sampling depth (solid line). The GRM acquisition is assumed to result from the presence of greigite as a magnetic signal carrier. Axial dipole field direction of either polarity indicated in subfigures B and C by blue and red lines, respectively. (For interpretation of the references to colour in this figure legend, the reader is referred to the web version of this article.)

magnetic carriers), or in the geochemical composition of the water body (chemical precipitation of magnetic minerals such as greigite). The ChRM declination and inclination for the U-channel material of the core NW09 (Fig. 5, Fig. 7B and C) generally indicate normal polarity (positive inclination; mean value of ~33°), although several short-term polarity reversals are also observed. During the AF demagnetisation, it was noticed that the mainly clastic sediment up-core ~15 m (Unit F) begins to occasionally acquire a new magnetisation at about 30–50 mT (Fig. 7D). This phenomenon is interpreted as a gyroremanent magnetisation (GRM), which may indicate the presence of greigite (e.g. Ron et al., 2007; Stephenson and Snowball, 2001). Greigite ($Fe_3S_4$) can grow authigenically under reducing conditions in the presence of sulphur and iron, e.g. in stagnant bottom waters or can be formed via post-depositional bacterial sulphate reduction (Berner, 1984; Reynolds et al., 1999). A post-sedimentary origin of the greigite would, however, introduce a secondary magnetisation and presumably hinder the stratigraphical interpretation of the magnetic orientations.

Investigation of the AMS properties at a core depth of 70–88 m shows variations of the magnetic anisotropy degree ($\kappa_1/\kappa_3$) in the range of 1.01–1.15, and a distinct shift from means of 1.04 below a depth of 84.60 m to 1.08 on average above (Fig. 8A). This increase reflects a better alignment of the magnetic fabric in the up-core section (Unit C) and indicates calmer sedimentation conditions, and coincides with the transition from till (Unit B) to proglacial lake deposits (Unit C).

The dips of the minimum principle axis $\kappa_3$ are broadly scattered from 0 to 85° (Fig. 8B), and is not in agreement with the expected dip range of 60–90° for typical horizontally bedded lacustrine sediments (Tarling and Hrouda, 1993). The heterogeneous dip pattern, especially in the proglacial part, might result from the influence of strong bottom currents (≥1 cm $s^{-1}$) or from the observed sediment deformation (Section 4.1). Post-sedimentary deformation (e.g. by later water escape, or artificially by rotary drilling, or less likely by hammering during U-channel extraction), can also not be excluded as the cause of scattered $\kappa_3$ dip directions. Considering that the primary magnetic fabric has most probably been distorted, that there is the potential for post-sedimentary greigite growth in Units F–J, and with the $\kappa_3$ dip scatter observed in Units B and C, it was not possible to derive reliable magnetostratigraphic information from the core.

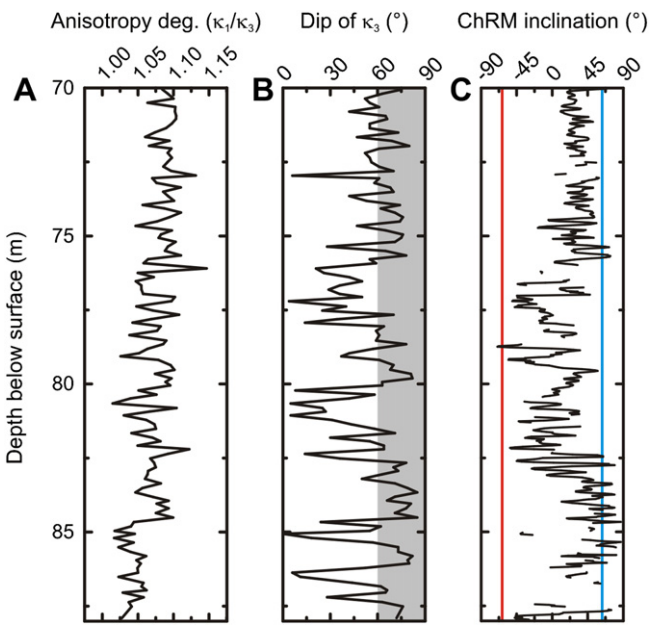


**Fig. 8.** A) Anisotropy degree of the magnetic susceptibility $\kappa_1/\kappa_3$. Note the striking increase of the mean anisotropy degree above a depth of ~84.60 m. This increase reflects a better alignment of the magnetic fabric in the up-core section and clearly marks the transition from till to a proglacial lake facies sedimentation regime. (B) Dip of the minimum principal axis of the susceptibility ellipsoid ($\kappa_3$). Grey area indicates expected dip range of the magnetic fabric (60–90°) for lacustrine sediments (e.g. Tarling and Hrouda, 1993). (C) Inclination of the characteristic remanent magnetisation (ChRM). Blue/red lines show expected normal/reversed inclination angles (at ~63.4°). (For interpretation of the references to colour in this figure legend, the reader is referred to the web version of this article.)

### 4.7. Luminescence dating

$D_e$ values and ages for OSL and IRSL are reported together with dosimetric data in Table 1 and illustrated in Fig. 9. The luminescence ages span from ~300 ka at the bottom of the core up to ~45 ka at the top, and IRSL and OSL ages are in agreement within errors above 60 m. Further down the core however, the chronologies diverge. Occasionally, the lower bleachability of the IRSL compared to the OSL signal has been used to explain such offset. However, the observed offset in ages is much larger than the one found in the bleaching experiment. Nevertheless, a difference in bleaching characteristics between the two signals clearly exists, and it is possible that turbid water conditions (i.e. from glacial meltwater) during transport could have exploited this disparity further and contribute to the divergence in ages.

Although quartz OSL is recognised as reliable for the dating of sediments (Murray and Olley, 2002), problems of underestimation have been reported for some samples of Eemian age or older (Lai, 2010; Lowick et al., 2010a; Murray et al., 2007; Timar et al., 2010). Debate is on-going regarding the reliability of quartz ages derived from a high dose linear region of the OSL dose response curve (Lai, 2010; Lowick et al., 2010b), as the success of the SAR protocol relies partly on isolating a signal that displays a single saturating exponential, and the additional linear response is not yet understood (Bøtter-Jensen et al., 2003; Wintle, 2008). Nonetheless, ages have been reported that are in agreement with independent dating that were derived from such a high dose linear region (Murray et al., 2008; Pawley et al., 2008). The linear part of the dose response is in fact most likely the early expression of a later saturating exponential that has been poorly characterised due to insufficient dose points (Lowick et al., 2010b). The quartz from Niederweningen displays this second saturating exponential but it has also undergone extensive investigation (Lowick and Preusser, 2011; Lowick et al., 2010b), and no indications were found to suggest that the age determination should not be robust.

With regard to the IRSL signal measured in feldspar, it is generally seen to saturate at much higher burial doses than quartz OSL and thus offers the potential to date further back in time. For this site however, the dose response of both IRSL and OSL (Fig. 2) rise to similar levels, although the $D_e$ values determined for IRSL are up to 50% higher than those for OSL in the same sample, and may itself be problematic. When fitting a luminescence dose response curve to a saturating exponential, Wintle and Murray (2006) recommend that only $D_e$ values that fall below 2D0 (a value used to characterise 85% saturation of the signal) should be considered reliable. Although the dose response from both minerals fitted better to a saturating exponential plus linear (SEPL), they were fitted to a single saturating exponential function in order to evaluate the proximity of $D_e$ values to saturation. While all values for quartz OSL remained at least 40% below 2D0, $D_e$ values for the IRSL were up to 40% above this point, and raise doubts concerning their reliability. 2D0 was about 340–450 Gy and almost all quartz $D_e$ values were below this value.

The characteristics of sample NWE 1 (91 m depth) were studied more closely as this was interpreted as Lower Freshwater Molasse bedrock (see Section 4.2). The settling procedure firstly obtained

**Table 1**
Data summary of luminescence dating of core NW09, showing mean sampling depth, the number of aliquots measured ($n$), concentration of dose rate relevant elements (K, Th, U), measured sediment moisture content ($M$), calculated sediment palaeo-water content (PW), dose rate ($D$), equivalent dose ($D_e$) for feldspar IRSL (Fsp) and quartz OSL (Qz), and resulting ages.

| Sample name | Depth (m) | $n_{IRSL}$ | $n_{OSL}$ | K (%) | Th (ppm) | U (ppm) | $M$ (wt%) | PW (%) | $D_{Fsp}$ (Gy ka$^{-1}$) | $D_{e\ Fsp}$ (Gy) | IRSL age (ka) | $D_{Qz}$ (Gy ka$^{-1}$) | $D_{e\ Qz}$ (Gy) | OSL age (ka) |
|---|---|---|---|---|---|---|---|---|---|---|---|---|---|---|
| NWE 24 | 3.45 | 3/3 | 3/3 | 1.81 ± 0.02 | 9.66 ± 0.35 | 2.65 ± 0.07 | 30.3 | 35 | 2.99 ± 0.31 | 130.5 ± 4.0 | 43.6 ± 4.4 | – | – | – |
| NWE 23 | 5.65 | 3/3 | 3/3 | 1.76 ± 0.02 | 9.86 ± 0.26 | 2.48 ± 0.03 | 30.9 | 35 | 2.90 ± 0.29 | 135.7 ± 3.5 | 46.8 ± 4.6 | – | – | – |
| NWE 22 | 10.58 | 3/3 | 3/3 | 1.78 ± 0.02 | 8.75 ± 0.25 | 2.30 ± 0.04 | 23.4 | 30 | 2.85 ± 0.27 | 294.0 ± 2.0 | 103 ± 10 | 2.87 ± 0.37 | 287.2 ± 20.8 | 114 ± 12 |
| NWE 21 | 11.55 | 3/3 | 3/3 | 1.79 ± 0.02 | 8.88 ± 0.31 | 2.54 ± 0.08 | 22.8 | 30 | 2.93 ± 0.29 | 354.5 ± 6.2 | 121 ± 12 | 2.75 ± 0.26 | 318.5 ± 11.4 | 123 ± 11 |
| NWE 20 | 12.50 | 3/3 | 3/3 | 1.75 ± 0.02 | 8.17 ± 0.17 | 2.56 ± 0.06 | 24.7 | 30 | 2.84 ± 0.27 | 303.3 ± 3.6 | 107 ± 10 | – | – | – |
| NWE 19 | 14.89 | 3/3 | 3/3 | 2.12 ± 0.02 | 11.13 ± 0.36 | 3.41 ± 0.08 | 22.6 | 30 | 3.61 ± 0.36 | 359.6 ± 5.0 | 99.7 ± 9.9 | 3.47 ± 0.36 | 292.7 ± 13.2 | 92.5 ± 8.3 |
| NWE 18 | 16.20 | 3/5 | 3/3 | 1.72 ± 0.02 | 9.04 ± 0.15 | 3.11 ± 0.03 | 22.7 | 30 | 3.04 ± 0.30 | 356.3 ± 5.7 | 117 ± 11 | 2.92 ± 0.29 | 272.5 ± 11.1 | 103 ± 9 |
| NWE 17.5 | 17.70 | 4/4 | 3/3 | 1.18 ± 0.02 | 6.27 ± 0.19 | 2.18 ± 0.02 | 10.3 | 30 | 2.12 ± 0.22 | 397.2 ± 9.2 | 187 ± 19 | – | – | – |
| NWE 17 | 19.55 | 5/5 | 3/3 | 1.32 ± 0.02 | 7.53 ± 0.09 | 2.43 ± 0.02 | 18.4 | 30 | 2.41 ± 0.25 | 420.9 ± 11.6 | 175 ± 18 | 2.34 ± 0.21 | 326.1 ± 9.2 | 156 ± 13 |
| NWE 16 | 24.26 | 4/4 | 3/3 | 1.47 ± 0.02 | 7.52 ± 0.31 | 2.42 ± 0.05 | 19.4 | 30 | 2.50 ± 0.33 | 440.1 ± 27.0 | 176 ± 20 | 2.50 ± 0.57 | 371.7 ± 56.3 | 170 ± 29 |
| NWE 15 | 29.25 | 3/5 | 3/3 | 1.34 ± 0.02 | 7.21 ± 0.15 | 2.37 ± 0.09 | 18.6 | 30 | 2.37 ± 0.28 | 420.9 ± 19.9 | 178 ± 20 | 2.38 ± 0.36 | 318.7 ± 27.4 | 155 ± 18 |
| NWE 14 | 32.46 | 5/5 | 3/3 | 1.34 ± 0.02 | 7.40 ± 0.20 | 2.51 ± 0.04 | 19.6 | 30 | 2.42 ± 0.25 | 531.1 ± 12.1 | 219 ± 22 | 2.31 ± 0.39 | 333.7 ± 34.7 | 159 ± 21 |
| NWE 13 | 35.24 | 5/5 | 3/3 | 1.38 ± 0.02 | 7.39 ± 0.17 | 2.35 ± 0.09 | 20.0 | 30 | 2.39 ± 0.28 | 472.8 ± 20.8 | 198 ± 21 | 2.34 ± 0.22 | 361.6 ± 11.9 | 173 ± 15 |
| NWE 12 | 38.50 | 3/3 | 3/3 | 1.34 ± 0.02 | 7.40 ± 0.15 | 2.47 ± 0.05 | 19.1 | 30 | 2.40 ± 0.24 | 508.5 ± 2.6 | 212 ± 21 | 2.41 ± 0.26 | 390.8 ± 18.6 | 188 ± 17 |
| NWE 11 | 40.30 | 5/6 | 3/3 | 1.40 ± 0.02 | 7.42 ± 0.30 | 2.45 ± 0.09 | 19.0 | 30 | 2.44 ± 0.29 | 475.9 ± 20.5 | 195 ± 21 | 2.43 ± 0.44 | 406.0 ± 45.6 | 191 ± 26 |
| NWE 10.5 | 42.90 | 4/4 | 3/3 | 1.32 ± 0.02 | 6.71 ± 0.32 | 2.35 ± 0.04 | 11.8 | 30 | 2.29 ± 0.26 | 476.8 ± 16.9 | 209 ± 22 | 2.28 ± 0.37 | 326.8 ± 32.3 | 164 ± 21 |
| NWE 10 | 45.32 | 4/6 | 3/3 | 1.06 ± 0.01 | 4.67 ± 0.12 | 1.91 ± 0.03 | 24.4 | 30 | 1.79 ± 0.20 | 486.9 ± 21.7 | 272 ± 29 | 1.54 ± 0.18 | 255.5 ± 16.8 | 174 ± 34 |
| NWE 9 | 48.53 | 3/6 | 3/3 | 1.20 ± 0.01 | 5.79 ± 0.39 | 2.17 ± 0.03 | 21.7 | 30 | 2.07 ± 0.22 | 548.2 ± 14.5 | 265 ± 28 | 1.94 ± 0.31 | 394.1 ± 37.4 | 219 ± 27 |
| NWE 8.5 | 51.08 | 4/4 | 3/3 | 1.36 ± 0.02 | 6.91 ± 0.16 | 2.36 ± 0.05 | 12.4 | 30 | 2.34 ± 0.24 | 545.9 ± 13.8 | 234 ± 24 | – | – | – |
| NWE 8 | 53.71 | 4/4 | 3/3 | 1.30 ± 0.01 | 6.94 ± 0.22 | 2.42 ± 0.02 | 19.8 | 30 | 2.31 ± 0.25 | 495.8 ± 15.5 | 215 ± 22 | – | – | – |
| NWE 7.5 | 57.53 | 4/4 | 3/3 | 1.44 ± 0.02 | 7.10 ± 0.12 | 2.38 ± 0.04 | 10.6 | 30 | 2.41 ± 0.27 | 592.4 ± 25.1 | 245 ± 26 | – | – | – |
| NWE 7 | 60.37 | 5/5 | 3/3 | 1.29 ± 0.02 | 6.89 ± 0.21 | 2.35 ± 0.04 | 16.8 | 30 | 2.28 ± 0.26 | 541.0 ± 22.4 | 237 ± 25 | 2.24 ± 0.23 | 391.0 ± 16.3 | 198 ± 17 |
| NWE 6.5 | 64.08 | 4/4 | 3/3 | 1.30 ± 0.02 | 6.97 ± 0.14 | 2.39 ± 0.05 | 7.1 | 30 | 2.30 ± 0.30 | 565.5 ± 35.3 | 246 ± 29 | – | – | – |
| NWE 6 | 69.41 | 5/5 | 3/3 | 1.17 ± 0.01 | 6.09 ± 0.29 | 2.46 ± 0.02 | 17.1 | 30 | 2.16 ± 0.23 | 601.6 ± 15.6 | 279 ± 29 | 1.77 ± 0.30 | 326.8 ± 35.3 | 175 ± 24 |
| NWE 5 | 73.84 | 4/4 | 3/3 | 1.16 ± 0.01 | 7.09 ± 0.13 | 2.57 ± 0.03 | 19.2 | 30 | 2.26 ± 0.23 | 541.9 ± 7.2 | 239 ± 24 | 2.04 ± 0.17 | 334.2 ± 6.9 | 172 ± 14 |
| NWE 4 | 77.82 | 4/4 | 3/3 | 1.11 ± 0.01 | 6.14 ± 0.14 | 2.48 ± 0.06 | 24.0 | 30 | 2.12 ± 0.22 | 533.2 ± 6.9 | 252 ± 26 | 1.98 ± 0.48 | 408.8 ± 66.2 | 224 ± 40 |
| NWE 3 | 80.70 | 4/4 | 3/3 | 1.18 ± 0.01 | 6.88 ± 0.14 | 2.49 ± 0.08 | 17.7 | 30 | 2.24 ± 0.23 | 512.7 ± 5.2 | 229 ± 23 | 1.97 ± 0.47 | 444.0 ± 69.9 | 230 ± 41 |
| NWE 2 | 86.76 | 5/5 | 3/3 | 1.22 ± 0.01 | 6.44 ± 0.08 | 2.63 ± 0.06 | 14.3 | 30 | 2.27 ± 0.25 | 614.9 ± 21.6 | 271 ± 29 | 2.09 ± 0.36 | 394.3 ± 42.5 | 201 ± 27 |
| NWE 1 | 91.35 | 4/4 | 5/5 | 2.87 ± 0.03 | 10.94 ± 0.19 | 2.20 ± 0.05 | 7.3 | 30 | 3.73 ± 0.42 | 879.2 ± 46.5 | 235 ± 23 | – | – | – |

very little polymineral fine grains from this sample and, following immersion in fluorosilicic acid for a week, the remaining quartz fraction appeared considerably larger than 4–11 μm and required securing with silicon spray to aliquots rather than settling with acetone. The IRSL signal was in saturation and therefore an age of 250 ka determined from the polymineral fraction can only be regarded as a minimum. The luminescence characteristics of the quartz fraction were also very different and are illustrated in Fig. 10. Signal intensity was very low, suggesting that this material has a young sedimentary history with little reworking (Preusser et al., 2006), and the signal was saturated at 400 Gy, unlike the overlying samples whose dose response continued to grow above 800 Gy. The luminescence characteristics of this sample fit very well with its interpretation as in-situ bedrock.

The IRSL chronology from 90 to 17 m (Units B to D) suggests deposition of sediment from ~270 to ~180 ka, thus through MIS 8 and 7. These units are however, interpreted as lacustrine cold-climate sediments deposited in the presence of a glacier and are expected to represent a rather short time interval due to the high sedimentation rates in such settings. Furthermore, the pollen record conflicts with deposition during interglacial conditions expected for MIS 7 (cf. Preusser et al., 2005). As a consequence, the IRSL ages do not agree with either sedimentology or palynology. On the other hand, the majority of the quartz OSL ages suggest that all of these units were deposited during MIS 6 and this is consistent with the other observations, especially the sedimentological evolution. Interestingly, IRSL and OSL show little difference in the distal glaciolacustrine samples (above Unit D1) and the offset is most pronounced in the proximal sediments containing dropstones (below Unit D1). As a consequence, the feldspar IRSL ages are interpreted as suffering incomplete bleaching of the signal prior to deposition, due to short distance transport in turbid water

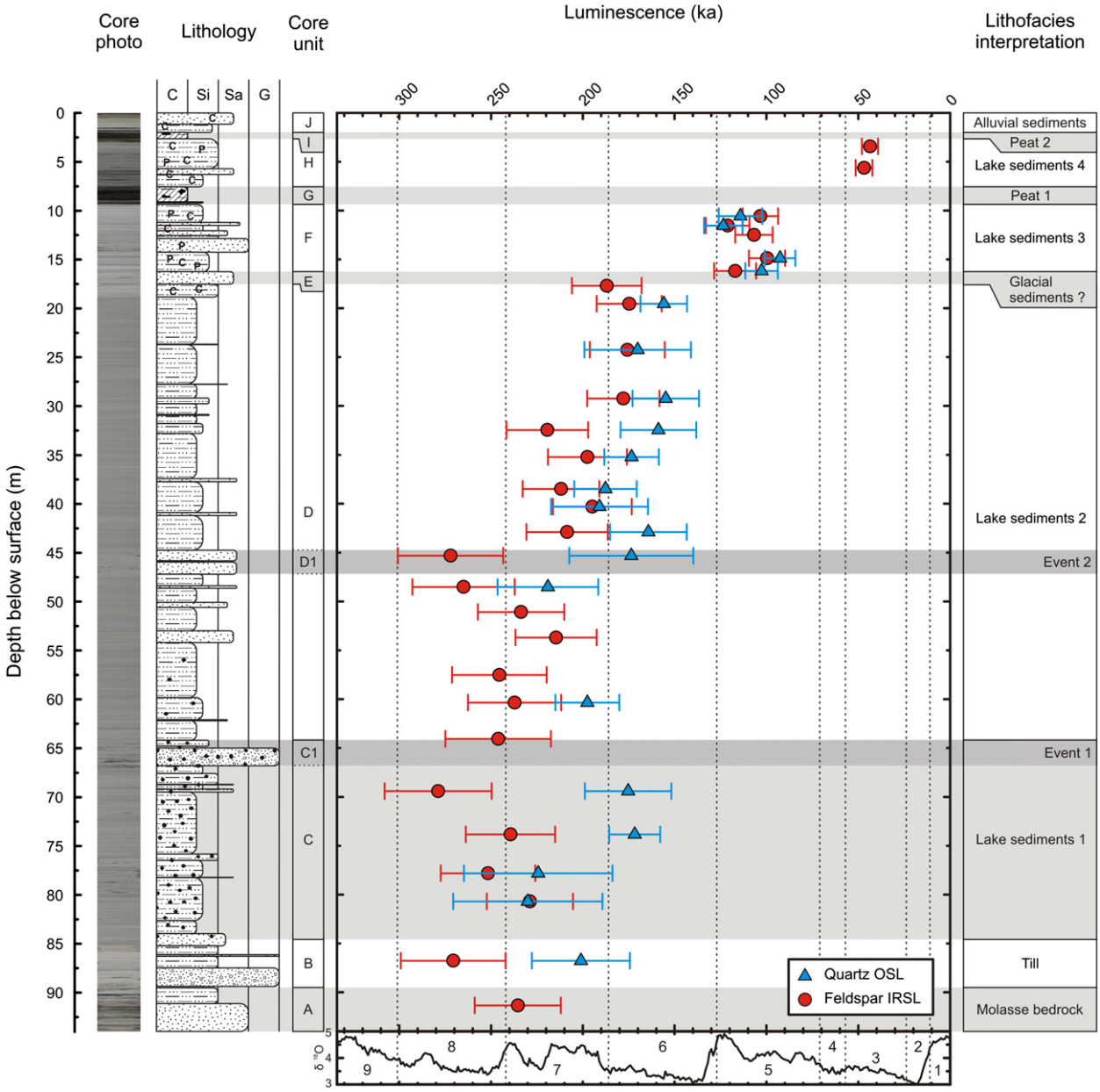


**Fig. 9.** Luminescence chronology of core NW09. Oxygen isotope curve at the bottom is LR04 stack by Lisiecki and Raymo (2005) with Marine Isotope Stages following Bassinot et al. (1994).

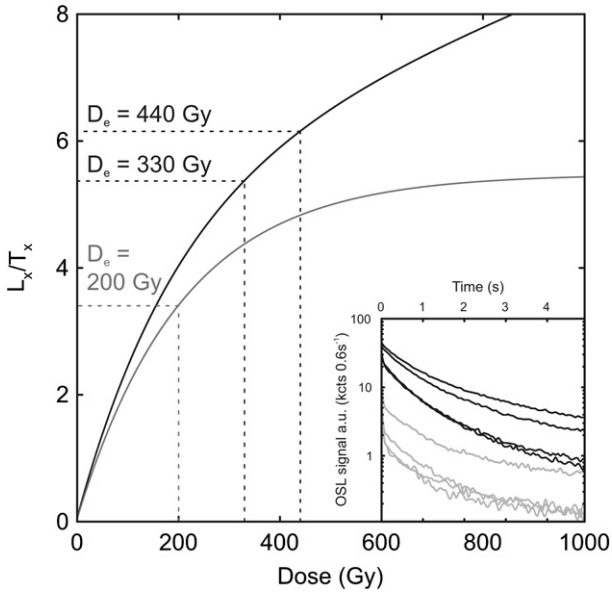


**Fig. 10.** Comparison of quartz OSL characteristics for sample NWE 1 (91 m depth) (grey lines) with that from overlying samples (black lines). Main figure shows the dose response curve from NWE 1 (average of four aliquots) with that of overlying samples NWE 3 and NWE 5 (two aliquots each), and is typical of all other samples. While the dose response of NWE 1 fits best to a single saturating exponential, all other samples are best described by a saturating exponential plus linear fit. Dashed lines indicate $D_e$ values determined for the three samples. Inset shows the OSL decay curves following a laboratory dose of 1150 Gy for all aliquots represented in the main figure (note log scale of *y*-axis).

suspension. This additional signal brings them closer to saturation which had already been recognised as a problem. The quartz OSL ages, although some of these also appear to be overestimated, are considered to more closely reflect the true age of deposition. From the available data, we infer an age of ~185 ka for the basal part of the sequence and deposition of the distal lake deposits (Unit D) is recorded until not later than ~150 ka.

For Unit F (9–16 m) above the unconformity (Unit E), but below the lower peat unit (Unit G), OSL ages span from 93 ± 8 to 124 ± 11 ka (mean 105 ± 12 ka) whereas the IRSL ages range between 100 ± 10 ka and 121 ± 12 ka (mean 109 ± 8 ka). Both data set suggest an age younger than Eemian (130–115 ka, cf. Preusser, 2004), and support an interpretation of the peat correlating, not with the Eemian, but with the second Early Würmian interstadial (MIS 5a) as suggested by the presence of *Osmunda* (see above). It is worth noting that the lake sediments above the peat (Unit H, not dated in this study) have identical mean ages of 71 ± 3 ka for both IRSL and OSL (Anselmetti et al., 2010). This age fits very well with the end of the second Early Würmian interstadial that is considered to have terminated just prior to 70 ka (cf. Preusser, 2004). IRSL ages between 3 and 6 m (upper part of Unit H) are 47 ± 5 ka and 44 ± 4 ka, respectively, and fit well with the age of the 'mammoth peat' reported in previous studies (Anselmetti et al., 2010; Hajdas et al., 2007; Preusser and Degering, 2007).

## 5. Discussion and conclusions

The seismic survey together with data of previous drill holes indicates a substantial fill of Quaternary sediments in Wehntal. Till and cross-bedded delta deposits are widespread below the present valley floor suggesting an ice marginal position in the past. Clear proof for a glacial advance from the Alps towards Niederweningen is indeed documented in the lower part of this sedimentary record. The fact that till rests directly on top of molasse bedrock indicates that the glacier either carved out a new basin into bedrock or at least completely eroded all previous Quaternary deposits (Fig. 11A). Meltdown of the ice is reflected by the lake sediments on top of the till, showing the transition from a proximal, drop-stone-dominated facies (Fig. 11B) towards a more distal, almost pure silt facies (Fig. 11C). The quartz OSL ages imply that the area became ice-free around 180 ka ago, i.e. during the early part of MIS 6. At first glance, it appeared that subsequent filling of the basin was continuous, and terminated in the deposition of peat. However, two breaks in sedimentation are observed and have major implications for the glaciation history of the area.

The first break is indicated by disturbed sediment structures at 17.60 m and is confirmed by a pronounced offset in both the OSL and IRSL ages, which indicate a disturbance between c. 150–140 ka, i.e. during the second part of MIS 6. The sediment just above the unconformity is almost free of pollen, slightly coarser and later shows a warming trend that is typical for Late Glacial conditions. A break in sedimentation at the same position, and at the same time, was reported by Anselmetti et al. (2010), about 330 m from the present drilling position. The prominent increase in shear strength below this horizon, as well as deformation structures, are found in both drill sites and occur within uniform silty lithologies. Shear-strength values then gradually decrease from the maximum downcore in the silty inorganic sediments to 50 m depth. These sedimentological and petrophysical patterns may reflect the grounding of ice, possibly of a cold-based glacier in the basin (Fig. 11D), which would explain both, the alteration of the sediment, together with the lack of glacial sediments associated with this ice advance. This glacier would have touched the former lake floor, partly eroding, deforming and consolidating the underlying lake sediments as expressed by the increased shear-strength values. Interestingly, Haeberli and Schlüchter (1987) have suggested a transformation from warm to cold-based glaciers at the end of the Last Glaciation in the Swiss lowlands, supporting our recent observations of the penultimate glacial cycle. Alternatively, the increased shear-strength values and deformation structures may also reflect lateral slumping or sliding, which would also enhance consolidation and which could furthermore explain the observed coarsening-up trend. However, no clear slump-induced features or overlying megaturbidites, which would be expected from a nearby slope or delta failure (Schnellmann et al., 2005), can be clearly recognised. A slump also would not explain the gradual downcore decrease in shear strength over tens of metres as it is observed below the critical horizon.

If the interpretation of subglacial deformations is correct, the NW09 record indicates two glacial advances into Wehntal during MIS 6 that extended beyond the limits of the Last Glaciation in the Swiss Lowlands. The first advance represents the main advance of the Beringen (Rissian) Glaciation, which reached several 10 km beyond Wehntal, and is attributed to MIS 6 based on preliminary IRSL dating (Graf, 2009; Preusser et al., 2011). Further, the Niederweningen record indicates that after this first advance, the ice melted back so far that no direct evidence of glacial input is recorded in the lake sediments. The second later advance probably represents a phase of new ice build-up and was of smaller extent, as it did not erode major parts of the previous basin fill. Two individual ice advances during the Beringen Glaciation have already been recorded in the Linth area, west of Lake Walen (Schindler, 2004) and also in south-western Germany (Miara et al., 1996). Moreover, the Saalian Glaciation in northern central Europe consists of two major glacial advances. The older and more extensive Drenthe stage has been dated to MIS 6 by OSL (Busschers et al., 2008). The second advance is older than Last Interglacial as inferred from the presence of Eemian pollen assemblages in lake deposits on

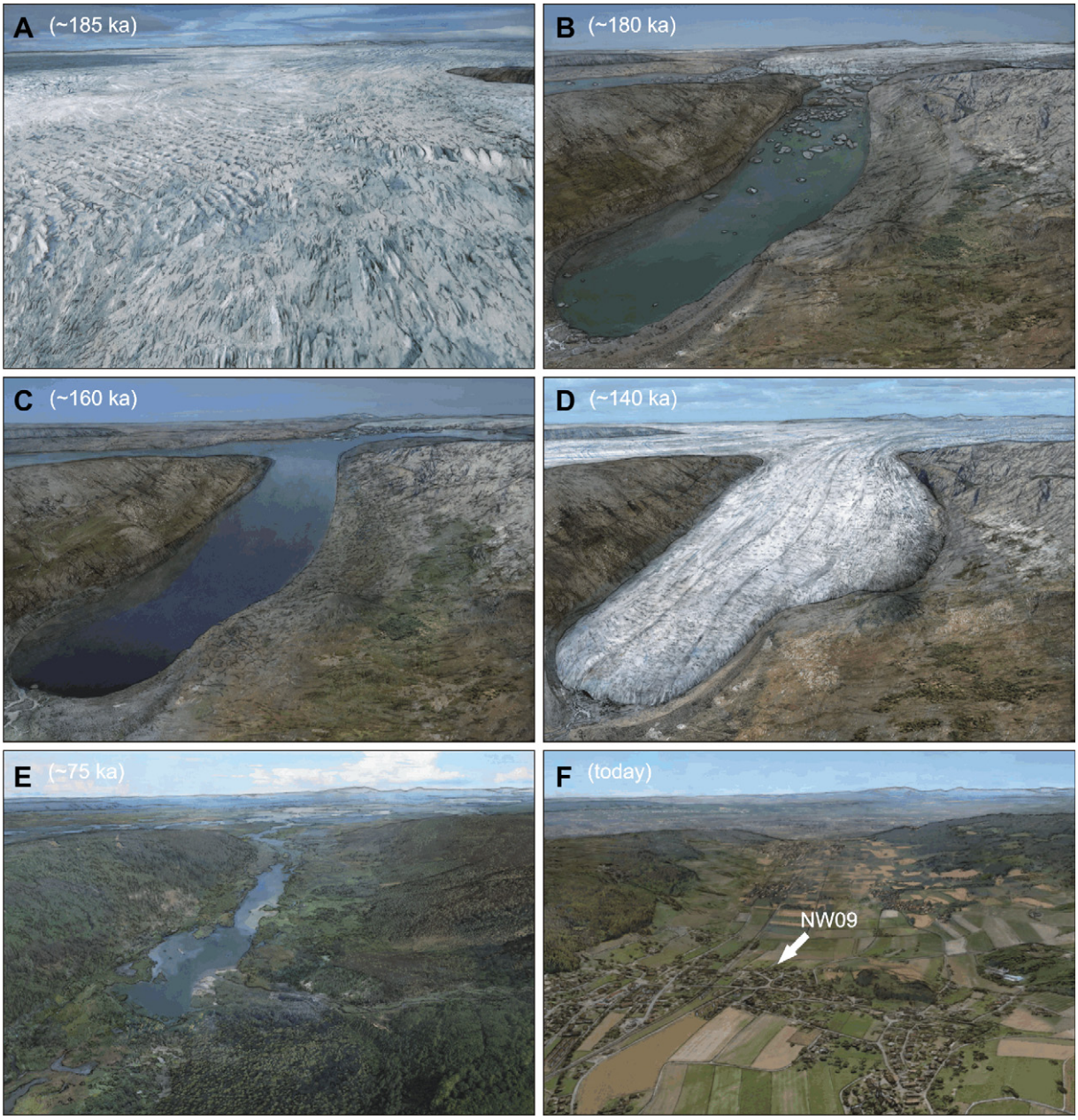


**Fig. 11.** Landscape reconstructions of the Wehntal site as recorded in core NW09. View along the main valley axis facing south-east. For orientation see Fig. 1. All figures are the property of the Mammutmuseum Niederweningen (www.mammutmuseum.ch). (A) Main advance of the Walensee Glacier during the Beringen Glaciation in early MIS 6. (B) Proglacial lake with drifting icebergs in the Wehntal caused by melting of the Walensee Glacier. (C) Connected proglacial lakes in the Glatt Valley (upper and middle) and Wehntal. (D) Second ice advance into the Wehntal during Late MIS 6. (E) Alder carr environment in the valley bottom with mixed forest vegetation at the valley flanks during the second Early Würmian interstadial (MIS 5a). (F) The recent Wehntal showing the village of Niederweningen and the NW09 drill site (arrow) in the foreground.

top of glacial sediments (cf. Litt et al., 2007). This Warthe stage was of slightly larger extent than the Last Glaciation (Weichsel) in northern Germany (cf. Ehlers et al., 2004). To summarise, the glacial dynamics of Wehntal are similar to those observed in other regions and therefore may hence reflect the response of glaciers to external climate forcing.

The second break in sedimentation in the NW09 record is indicated by the absence of an interval with typical thermophile pollen representing the last interglacial (Eemian). The luminescence dating and palynology point towards a correlation of the Unit G peat with the second Early Würmian interstadial (Odderade or Ufhusen, MIS 5a; Fig. 11E), and suggests a sedimentary gap of ~30 ka. It was not possible to determine if the gap represents either no deposition or an erosional phase.

This study identified in the lower lake deposits a large amount of reworked pollen and recommends cautions against interpreting the pollen content of lake deposits with a high detrital input. Previous reports based on pollen records of an older interglacial at this site appear unfounded.

## Acknowledgements

A. Dehnert and H.A. Kemna were financially supported by the Swiss National Science Foundation (project no. 200021-125304 and

200020-129977 to H. Furrer). We are indebted to J. Reitner and C. Spötl for their valuable reviews and thank U. Fischer for his comments. We thank the National Cooperative for the Disposal of Radioactive Waste (Nagra) for financing S.E. Lowick and supporting the seismic survey in 2008. We further acknowledge financial and operational support from the Promotion Society and Foundation Mammutmuseum Niederweningen (R. Hauser, F. Wittwer) and from Bucher Industries Niederweningen. H. Mayrhofer, director of the Institute of Plant Science of Karl-Franzens-University of Graz, is thanked for supporting the preparation of the pollen samples in his laboratories. A. Gilli supported analysis in the Limnology Laboratory of the ETH Zurich. I. Brunner (Eawag) measured the geochemistry. Gamma spectrometry was carried out by S. Szidat, Department of Chemistry and Biochemistry, University of Bern. The drilling company Stump ForaTec AG provided excellent core material.

## Appendix. Supplementary data

Supplementary data associated with this article can be found, in the online version, at doi:10.1016/j.quascirev.2011.12.015.

## References


Aitken, M.J., 1985. Thermoluminescence Dating. Academic Press, New York.

Anselmetti, F.S., Drescher-Schneider, R., Furrer, H., Graf, H.R., Lowick, S.E., Preusser, F., Riedi, M.A., 2010. A ~180,000 years sedimentation history of a perialpine overdeepened glacial trough (Wehntal, N-Switzerland). Swiss Journal of Geosciences 103, 345–361.

Auclair, M., Lamonthe, M., Huot, S., 2003. Measurement of anomalous fading for feldspar IRSL using SAR. Radiation Measurements 37, 487.

Bøtter-Jensen, L., McKeever, S.W.S., Wintle, A.G., 2003. Optically Stimulated Luminescence Dosimetry. Elsevier, Amsterdam.

Ballarini, M., Wallinga, J., Wintle, A.G., Bos, J.A.A., 2007. A modified SAR protocol for optical dating of individual grains from young quartz samples. Radiation Measurements 42, 360–369.

Bassinot, F.C., Labeyrie, L.D., Vincent, E., Quidelleur, X., Shackleton, N.J., Lancelot, Y., 1994. The astronomical theory of climate and the age of the Brunhes-Matuyama magnetic reversal. Earth and Planetary Science Letters 126, 91–108.

de Beaulieu, J.-L., Andrieu-Ponel, V., Reille, M., Grüger, E., Tzedakis, C., Svobodova, H., 2001. An attempt at correlation between the Velay pollen sequence and the Middle Pleistocene stratigraphy from central Europe. Quaternary Science Reviews 20, 1593–1602.

Berner, R.A., 1984. Sedimentary pyrite formation: an update. Geochimica et Cosmochimica Acta 48, 605–615.

Bini, A., Buoncristiani, J.-F., Couterrand, S., Ellwanger, D., Felber, M., Florineth, D., Graf, H.R., Keller, O., Kelly, M.A., Schlüchter, C., Schoeneich, P., 2009. Die Schweiz während des letzteiszeitlichen Maximums (LGM) 1:500 000. Bundesamt für Landestopografie swisstopo, Wabern.

Birks, H.J.B., 1986. Numerical zonation, comparison and correlation of Quaternary pollen-stratigraphical data. In: Berglund, B.E., Ralska-Jasiewiczowa, M. (Eds.), Handbook of the Holocene Palaeoecology and Palaeohydrology. Wiley & Sons, Chichester, pp. 743–774.

Bitterli-Dreher, P., Graf, H.R., Naef, H., Diebhold, P., Matousek, F., Burger, H., Pauli-Gabi, T., 2007. Blatt 1070 Baden. Erläuterungen zum Geologischen Atlas der Schweiz 1 (25'000 120), 1–152.

Blüm, W., Wyssling, G., 2007. Ur-Sihl und Richterswiler Gletschertal - Quellen und Grundwasservorkommen zwischen Sihltal und Zürichsee. Baudirektion Kanton Zürich, AWEL Amt für Abfall, Wasser, Energie und Luft, Zürich.

Blair, M.W., Yukihara, E.G., McKeever, S.W.S., 2005. Experiences with single aliquot OSL procedures using coarse-grain feldspars. Radiation Measurements 39, 361–374.

Busschers, F.S., van Balen, R.T., Cohen, K.M., Kasse, C., Weerts, H.J.T., Wallinga, J., Bunnik, F.P.M., 2008. Response of the Rhine–Meuse fluvial system to Saalian ice-sheet dynamics. Boreas 37, 377–398.

Calvert, S.E., Thode, H.G., Yeung, D., Karlin, R.E., 1996. A stable isotope study of pyrite formation in the Late Pleistocene and Holocene sediments of the Black Sea. Geochimica et Cosmochimica Acta 60, 1261–1270.

Chowdhury, A.H., Noble, J.P.A., 1996. Organic carbon and pyrite sulphur relationships as evidences of bottom water conditions of sedimentation, Albert formation fine-grained lacustrine sediments, New Brunswick, Canada. Marine and Petroleum Geology 13, 79–90.

Cohen, A.S., 2003. Paleolimnology: The History and Evolution of Lake Systems. Oxford University Press, Oxford.

Collinson, J., Mountney, N., Thompson, D., 2006. Sedimentary Structures, third ed. Terra Publishing, Harpenden.

Cushing, E.J., 1964. Application of the code of stratigraphie nomenclature to pollen stratigraphy. In: Berglund, B.E., Ralska-Jasiewiczowa, M. (Eds.), Handbook of the Holocene Palaeoecology and Palaeohydrology. Wiley & Sons, Chichester, p. 869. 1986.

Dürst Stucki, M., Reber, R., Schlunegger, F., 2010. Subglacial tunnel valleys in the Alpine foreland: an example from Bern, Switzerland. Swiss Journal of Geosciences 103, 363–374.

Dehnert, A., Preusser, F., Kramers, J.D., Akçar, N., Kubik, P.W., Reber, R., Schlüchter, C., 2010. A multi-dating approach applied to proglacial sediments attributed to the most extensive Glaciation of the Swiss Alps. Boreas 39, 620–632.

Drescher-Schneider, R., 2000. Die Vegetations- und Klimaentwicklung im Riß/Würm-Interglazial und im Früh- und Mittelwürm in der Umgebung von Mondsee. Ergebnisse der pollenanalytischen Untersuchungen. In: van Husen, D. (Ed.), Klimaentwicklung im Riss/Würm Interglazial (Eem) und Frühwürm (Sauerstoffisotopenstufe 6–3) in den Ostalpen, Wien, pp. 39–92.

Drescher-Schneider, R., Jacquat, C., Schoch, W., 2007. Palaeobotanical investigations at the mammoth site of Niederweningen (Kanton Zürich). Switzerland. Quaternary International 164–165, 113–129.

Ehlers, J., Eissmann, L., Lippstreu, L., Stephan, H.-J., Wansa, S., 2004. Pleistocene glaciations of North Germany. In: Ehlers, J., Gibbard, P.L. (Eds.), Quaternary Glaciations – Extent and Chronology Part I: Europe. Elsevier, Amsterdam, pp. 135–146.

Erdtmann, G., 1934. Über die Verwendung von Essigsäureanhydrid bei Pollenuntersuchungen. Svensk Botanisk Tidskrift 28, 354–358.

Freimoser, M., Locher, T., 1980. Gedanken zur pleistozänen Landschaftsgeschichte im nördlichen Teil des Kantons Zürich aufgrund hydrogeologischer Untersuchungen. Eclogae Geologicae Helvetiae 73, 251–270.

Furrer, H., Graf, H.R., Mäder, A., 2007. The mammoth site of Niederweningen, Switzerland. Quaternary International 164-165, 85–97.

Geyh, M.A., Müller, H., 2005. Numerical $^{230}$Th/U dating and a palynological review of the Holsteinian/Hoxnian Interglacial. Quaternary Science Reviews 24, 1861–1872.

Grüger, E., 1979. Spätriß, Riß/Würm und Frühwürm am Samerberg in Oberbayern – ein vegetationsgeschichtlicher Beitrag zur Gliederung des Jungpleistozäns. Geologica Bavarica 80, 5–64.

Grüger, E., Schreiner, A., 1993. Riß/Würm- und würmzeitliche Ablagerungen im Wurzacher Becken (Rheingletschergebiet). Neues Jahrbuch für Geologie und Paläontologie - Abhandlungen 189, 81–117.

Graf, H.R., 1993. Die Deckenschotter der zentralen Nordschweiz. Ph.D. thesis, ETH, Zürich.

Graf, A.A., Strasky, S., Ivy-Ochs, S., Akçar, N., Kubik, P.W., Burkhard, M., Schlüchter, C., 2007. First results of cosmogenic dated pre-Last Glaciation erratics from the Montoz area, Jura Mountains, Switzerland. Quaternary International 164-165, 43–52.

Graf, H.R., 2009. Stratigraphie von Mittel- und Spätpleistozän in der Nordschweiz. Beiträge zur Geologischen Karte der Schweiz 168, 1–198.

Graf, H.R., Müller, B.U., 1999. Das Quartär: Die Epoche der Eiszeiten. In: Bolliger, T. (Ed.), Geologie des Kantons Zürich. Ott Verlag, Thun, pp. 71–95.

Haeberli, W., Schlüchter, C., 1987. Geological evidence to constrain modelling of the Late Pleistocene Rhonegletscher (Switzerland). In: Waddington, E.D., Walder, J.S. (Eds.), The Physical Basis of Ice Sheet Modelling. IAHS Press, Vancouver, pp. 333–346.

Hajdas, I., Bonani, G., Furrer, H., Mäder, A., Schoch, W., 2007. Radiocarbon chronology of the mammoth site at Niederweningen, Switzerland: results from dating bones, teeth, wood, and peat. Quaternary International 164-165, 98–105.

Hajdas, I., Michczyński, A., Bonani, G., Wacker, L., Furrer, H., 2009. Dating of bones near the limit of the radiocarbon dating method: study case mammoth from Niederweningen, ZH Switzerland. Radiocarbon 51, 675–680.

Haldimann, P.A., 1978. Quartärgeologische Entwicklung des mittleren Glattals (Kt.Zürich). Eclogae Geologicae Helvetiae 71, 347–355.

Hantke, R., 1978. Eiszeitalter – Die jüngste Erdgeschichte der Schweiz und ihrer Nachbargebiete. Ott Verlag AG, Thun.

Huntley, D.J., Lamonthe, M., 2001. Ubiquity of anomalous fading in K-feldspars and the measurement and correction for it in optical dating. Canadian Journal of Earth Sciences 38, 1093–1106.

van Husen, D., 2004. Quaternary glaciations in Austria. In: Ehlers, J., Gibbard, P.L. (Eds.), Quaternary Glaciations – Extent and Geochronology Part I: Europe. Elsevier, Amsterdam, pp. 1–13.

Jelínek, V., Kropáček, V., 1978. Statistical processing of anisotropy of magnetic susceptibility measured on groups of specimens. Studia Geophysica et Geodaetica 22, 50–62.

Jenny, V., de Quervain, F., 1961. Untersuchungen von Kalk- und Dolomitgehalt an Sanden quartärer Ablagerungen der Nordostschweiz. 2. Teil. Schweizerische mineralogische und petrographische Mitteilungen 41, 471–480.

Jordan, P., 2010. Analysis of overdeepened valleys using the digital elevation model of the bedrock surface of Northern Switzerland. Swiss Journal of Geosciences 103, 375–384.

Jordan, P., Schwab, M., Schuler, T., 2008. Digitales Höhenmodell – Am Beispiel der Felsoberfläche der Nordschweiz. GWA – Gas Wasser Abwasser 6/08, 443–449.

Küttel, M., 1989. Züge der jungpleistozänen Vegetations- und Landschaftsgeschichte der Zentralschweiz. Revue de Paléobiologie 8, 525–614.

Keller, O., Krayss, E., 2005a. The Rhine-Linth glacier during the last glacial maximum – part 2: dating and models of the Rhine-Linth glaciation. Climate reconstructions. Vierteljahrsschrift der Naturforschenden Gesellschaft in Zürich 150, 69–85.

Keller, O., Krayss, E., 2005b. The Rhine-Linth glacier in the last Glacial maximum –part 1: introduction. Building-up and retreat of the Rhine-Linth glacier during the upper Wurm. Vierteljahrsschrift der Naturforschenden Gesellschaft in Zürich 150, 19–32.
Kirschvink, J.L., 1980. The least-squares line and plane and the analysis of palaeomagnetic data. Geophysical Journal of the Royal Astronomical Society 62, 699–718.
Klasen, N., Fiebig, M., Preusser, F., Radtke, U., 2006. Luminescence properties of glaciofluvial sediments from the Bavarian Alpine Foreland. Radiation Measurements 41, 866–870.
Lai, Z., 2010. Chronolgy and the upper dating limit for loess samples from Luochuan section in the Chinese Loess Plateau using quartz OSL SAR protocol. Journal of Asian Earth Sciences 37, 176–185.
Lamonthe, M., Auclair, M., Hamzaoui, C., Huot, S., 2003. Towards a prediction of long-term anomalous fading of feldspar IRSL. Radiation Measurements 37, 493.
Lang, A., 1892. Geschichte der Mammutfunde. Ein Stück Geschichte der Paläontologie, nebst einem Bericht über den schweizerischen Mammutfund in Niederweningen 1890/91. Neujahrsblatt der Naturforschenden Gesellschaft in Zürich 44, 2–35.
Lisiecki, L.E., Raymo, M.E., 2005. A Pliocene–Pleistocene stack of 57 globally distributed benthic $d^{18}O$ records. Paleoceanography 20, PA1003.
Litt, T., Behre, K.-E., Meyer, K.-D., Stephan, H.-J., Wansa, S., 2007. Stratigraphical terms for the quaternary of the North German Glaciation area. E&G Quaternary Science Journal 56, 7–65.
Lowick, S.E., Preusser, F., 2011. Investigating age underestimation in the high dose region of optically stimulated luminescence using fine grain quartz. Quaternary Geochronology 6, 33–41.
Lowick, S.E., Preusser, F., Pini, R., Pavazzi, C., 2010a. Underestimation of fine grain quartz OSL dating towards the Eemian: comparison with palynostratigraphy from Azzano Decimo, northeastern Italy. Quaternary Geochronology 5, 583–590.
Lowick, S.E., Preusser, F., Wintle, A.G., 2010b. Investigating quartz optically stimulated luminescence dose-response curves at high doses. Radiation Measurements 45, 975–984.
Müller, U., 2001. Die vegetations- und Klimaentwicklung im jüngeren Quartär anhand ausgewählter Profile aus dem südwestdeutschen Alpenvorland. Tübinger Geowissenschaftliche Arbeiten D 7, 1–118.
Miara, S., Zoller, L., Rogner, K., Rousseau, D.D., 1996. Quaternary exposures near Baltringen/Riss and the stratigraphic division of the Riss-complex – new stratigraphical, pedological and geochronological aspects. Zeitschrift für Geomorphologie 40, 209–226.
Murray, A.S., Olley, J.M., 2002. Precision and accuracy in the optically stimulated luminescence dating of sedimentary quartz: a status review. Geochronometria 21, 1–16.
Murray, A.S., Wintle, A.G., 2000. Luminescence dating of quartz using an improved single-aliquot regenerative-dose protocol. Radiation Measurements 32, 57–73.
Murray, A.S., Svendsen, J.I., Mangerud, J., Astakhov, V.I., 2007. Testing the accuracy of quartz OSL dating using a known-age Eemian site on the river Sula, northern Russia. Quaternary Geochronology 2, 102–109.
Murray, A., Buylaert, J.-P., Henricksen, M., Svendsen, J.-I., Mangerud, J., 2008. Testing the reliability of quartz OSL ages beyond the Eemian. Radiation Measurements 43, 776–780.
Pawley, S.M., Bailey, R.M., Rose, J., Moorlock, B.S.P., Hamblin, R.J.O., Booth, S.J., Lee, J.R., 2008. Age limits on Middle Pleistocene glacial sediments from OSL dating north Norfolk. UK. Quaternary Science Reviews 27, 1363–1377.
Peckmann, J., Reimer, A., Luth, U., Luth, C., Hansen, B.T., Heinicke, C., Hoefs, J., Reitner, J., 2001. Methane-derived carbonates and authigenic pyrite from the northwestern Black Sea. Marine Geology 177, 129–150.
Pini, R., Ravazzi, C., Donegana, M., 2009. Pollen stratigraphy, vegetation and climate history of the last 215 ka in the Azzano Decimo core (plain of Friuli, northeastern Italy). Quaternary Science Reviews 28, 1268–1290.
Preusser, F., 2004. Towards a chronology of the Late Pleistocene in the northern Alpine Foreland. Boreas 33, 195–210.
Preusser, F., Degering, D., 2007. Luminescence dating of the Niederweningen mammoth site. Switzerland. Quaternary International 164-165, 106–112.
Preusser, F., Kasper, H.U., 2001. Comparison of dose rate determination using high-resolution gamma spectrometry and inductively coupled plasma - mass spectrometry. Ancient TL 19, 19–23.
Preusser, F., Drescher-Schneider, R., Fiebig, M., Schlüchter, C., 2005. Re-interpretation of the Meikirch pollen record, Swiss Alpine Foreland, and implications for Middle Pleistocene chronostratigraphy. Journal of Quaternary Science 20, 607–620.
Preusser, F., Ramseyer, K., Schlüchter, C., 2006. Characterisation of low luminescence intensity quartz from Westland, New Zealand. Radiation Measurements 41, 871–877.
Preusser, F., Reitner, J.M., Schlüchter, C., 2010. Distribution, geometry, age and origin of overdeepened valleys and basins in the Alps and their foreland. Swiss Journal of Geosciences 103, 407–426.
Preusser, F., Graf, H.R., Keller, O., Krayss, E., Schlüchter, C., 2011. Quaternary glaciation history of northern Switzerland. E&G Quaternary Science Journal 60, 282–305.
Psenner, R., 1983. Die Entstehung von Pyrit in rezenten Sedimenten des Piburger Sees. Aquatic Sciences - Research Across Boundaries 45, 219–232.
Pugin, A., 1988. Carte des isohypses de la base des sédiments du Quaternaire en Suisse occidentale, avec quelques commentaires. In: Geologische Berichte, vol. 3. Landeshydrogeologie und -geologie, Bern, p. 20.
Reynolds, R.L., Rosenbaum, J.G., van Metre, P., Tuttle, M., Callender, E., Goldin, A., 1999. Greigite ($Fe_3S_4$) as an indicator of drought – the 1912–1994 sediment magnetic record from White Rock Lake, Dallas, Texas, USA. Journal of Paleolimnology 21, 193–206.
Ron, H., Nowaczyk, N.R., Frank, U., Schwab, M.J., Naumann, R., Striewski, B., Agnon, A., 2007. Greigite detected as dominating remanence carrier in Late Pleistocene sediments, Lisan formation, from Lake Kinneret (Sea of Galilee), Israel. Geophysical Journal International 170, 117–131.
Schindler, C., 2004. Zum Quartär des Linthgebiets zwischen Luchsingen, dem Walensee und dem Zürcher Obersee. Beiträge zur Geologischen Karte der Schweiz 169, 1–159.
Schlüchter, C., 1979. Übertiefte Talabschnitte im Berner Mittelland zwischen Alpen und Jura (Schweiz). Eiszeitalter und Gegenwart 29, 101–113.
Schlüchter, C., 1988a. Neue geologische Beobachtungen bei der Mammutfundstelle in Niederweningen (Kt. Zürich). Vierteljahrsschrift der Naturforschenden Gesellschaft in Zürich 133, 99–108.
Schlüchter, C., 1988b. A non-classical summary of the Quaternary stratigraphy of the northern Alpine Foreland of Switzerland. Bulletin de la Société neuchâteloise de Géographie 32/33, 143–157.
Schlüchter, C., 1989a. The most complete Quaternary record of the Swiss Alpine Foreland. Palaeogeography, Palaeoclimatology, Palaeoecology 72, 141–146.
Schlüchter, C., 1989b. Thalgut: Ein umfassendes eiszeitstratigraphisches Referenzprofil im nördlichen Alpenvorland. Eclogae Geologicae Helvetiae 82, 277–284.
Schlüchter, C., 1994. Das Wehntal – Eine Schlüsselregion der Eiszeitenforschung. Jahrheft des Zürcher Unterländer Museumsvereins 28, 4–25.
Schlüchter, C., 2004. The Swiss glacial record - a schematic summary. In: Ehlers, J., Gibbard, P.L. (Eds.), Quaternary Glaciations – Extent and Chronology Part I: Europe. Elsevier, Amsterdam, pp. 413–418.
Schnellmann, M., Anselmetti, F.S., Giardini, D., McKenzie, J.A., 2005. Mass movement-induced fold-and-trust belt structures in unconsolidated sediments in Lake Lucern (Switzerland). Sedimentology 52, 271–289.
Sidler, C., 1988. Signification de la palynologie appliquée aux sédiments détritiques et organogènes du Pléistocène supérieur: Eem-Tardiglaciaire würmien et de l'Holocène entre Zoug, Zurich et Baden (Suisse). Mitteilungen aus dem geologischen Institut der Eidgenössischen Technischen Hochschule und der Universität Zürich – Neue Folge 280, 1–217.
Stephenson, A., Snowball, I.F., 2001. A large gyromagnetic effect in greigite. Geophysical Journal International 145, 570–575.
Stockmarr, J., 1971. Tablets with spores used in absolute pollen analysis. Pollen Spores 13, 615–621.
Tarling, D.H., Hrouda, F., 1993. The Magnetic Anisotropy of Rocks. Chapman and Hall, London.
Thiel, C., Coltorti, M., Tsukamoto, S., Frechen, M., 2010. Geochronology for some key sites along the coast of Sardinia (Italy). Quaternary International 222, 36–47.
Timar, A., Vandenberghe, D., Panaiotu, E.C., Panaiotu, C.G., Necula, C., Cosma, C., Van den Haute, P., 2010. Optical dating of Romanian loess using fine-grained quartz. Quaternary Geochronology 5, 143–148.
Wegmüller, S., 1992. Vegetationsgeschichtliche und stratigraphische Untersuchungen an Schieferkohlen des nördlichen Alpenvorlandes. Denkschriften der Schweizerischen Akademie der Naturwissenschaften 102, 1–82.
Welten, M., 1982. Pollenanalytische Untersuchungen im Jüngeren Quartär des nördlichen Alpenvorlandes der Schweiz. Beiträge zur Geologischen Karte der Schweiz 156, 1–174.
Welten, M., 1988. Neue pollenanalytische Ergebnisse über das Jüngere Quartär des nördlichen Alpenvorlandes der Schweiz (Mittel- und Jungpleistozän). Beiträge zur Geologischen Karte der Schweiz 162, 1–40.
Wildi, W., 1984. Isohypsenkarte der quartären Felstäler in der Nord- und Ostschweiz, mit kurzen Erläuterungen. Eclogae Geologicae Helvetiae 77, 541–551.
Wintle, A.G., 1973. Anomalous fading of thermoluminescence in mineral samples. Nature 245, 143–144.
Wintle, A.G., 2008. Luminescence dating: where it has been and where it is going. Boreas 37, 471–482.
Wintle, A.G., Murray, A.S., 2006. A review of quartz optically stimulated luminescence characteristics and their relevance in single-aliquot regeneration dating protocols. Radiation Measurements 41, 369–391.
Wyssling, G., 2002. Die Ur-Sihl floss einst ins Reusstal. Zur Geologie des Sihltals zwischen Schindellegi und Sihlbrugg. Verein ProSihltal 52, 1–14.
Wyssling, L., Wyssling, G., 1978. Interglaziale See-Ablagerungen in einer Bohrung bei Uster (Kanton Zürich). Eclogae Geologicae Helvetiae 71, 357–375.

**Supplementary figure.** Photographs of all lithotypes identified in core NW09. **A** Upper Freshwater Molasse bedrock, with topping palaeo-soil; **B** typical subaqueous diamiction (waterlain till); **C** laminated fine grained proglacial lake sediments with ice-rafted debris; **D** massive dropstone layer (Event 1) at the top of proglacial lake-sediment sequence; **E** clayey to silty lake sediments with characteristic mottled lamination; **F** weakly laminated sandy interbedding (Event 2); **G** silty to sandy lake sediments with lateral debris input; **H** laminated pyrite-rich silt and some sand, with some macroscopic plant remains (e.g. in the upper bluish part of photograph); **I** peat deposit with interbedded detrital silt patches; **J** silty lake sediments with small organic remains; **K** peat layer with well preserved plant remains ('mammoth peat'); **L** sandy alluvial sediments with organic remains and typical Fe-oxidation spots.